KLOE Note 213
August 2006

Fit to the $\pi^0\pi^0\gamma$ Dalitz plot

S. Giovannella, S. Miscetti

INFN - Laboratori Nazionali di Frascati

Abstract

In this note we show a new study of the events with a $\pi^0\pi^0\gamma$ final state collected at $\sqrt{s} \sim M_\phi$. Being $M_{\pi\pi}$ the dipion invariant mass, the process $e^+e^- \to \pi^0\pi^0\gamma$ is dominated by the not resonant $\rho \to \omega\pi$ mediated production for $M_{\pi\pi} < 700$ MeV, while for higher $M_{\pi\pi}$ values the radiative ϕ decay to a low mass scalar meson is the dominant mechanism. The novelty of the analysis presented here consists in avoiding the event-by-event separation of the two production processes and in extracting their characteristics by fitting, with different models, the Dalitz plot of these events. Fit results for the Kaon Loop and No Structure models are reported in detail. A comparison with the KLOE measurement in the $\pi^+\pi^-\gamma$ final state is also shown.

1 Introduction

The radiative decay $\phi \to S\gamma$, where S is one of the light scalar meson $\sigma(600)$, $f_0(980)$ or $a_0(980)$, can be detected in KLOE by looking at the $\pi^+\pi^-\gamma$, $\pi^0\pi^0\gamma$, $\eta\pi^0\gamma$ and $K\overline{K}\gamma$ final states. Searches for this kind of processes for the first three decay modes have been already published by our experiment [1, 2, 3]. The search for $K\overline{K}\gamma$, which is statistically limited, is instead being planned with the whole sample of 2.5 fb^{-1}. In this note, we show a new analysis method to extract the light meson parameters in the $\pi^0\pi^0\gamma$ channel which overseeds the one previously published, based on 145 pb^{-1} collected at $\sqrt{s} \sim M_\phi$. The final state into consideration can be produced either by the radiative ϕ decay to $[\sigma(600) + f_0(980)]\gamma$ ($S\gamma$) or by the Vector Meson Dominance (VMD) process $e^+e^- \to \rho \to \omega\pi^0$ ($\omega\pi$). In Fig. 1.top the expected Dalitz plot from Montecarlo is shown for these two production mechanisms. As Dalitz plot variables we use the invariant mass of the two pions, $M_{\pi\pi}$, and the invariant mass of a π^0 and the bachelor photon, $M_{\pi\gamma}$. Two entries per event are used for the two possible $\pi^0\gamma$ combinations. In Fig. 1.bottom-left the Montecarlo $M_{\pi\pi}$ distribution of the two processes shows the relative size of the production cross section. It is clear that the region above 700 MeV is dominated by the radiative ϕ decay to scalars while the region below is VMD dominated. The main difference with the old published analysis is summarized in the following points:

1. **π^0 pairing algorithm**
   We now pair photons to π^0's in a way which is independent from the process into consideration and does not require any constraint on the masses of the intermediate state of the decay (as for instance the ω meson). The new algorithm depends only on the photon energies after the kinematic fitting which imposes the 4-momentum conservation of the five photons to the center of mass energy [4].

2. **Dalitz plot density**
   The high statistics collected in 2001-2002 data taking allows us to study the density in the Dalitz plot instead of a single invariant mass combination. In Ref. [4] we have subdivided the events in two categories, $\omega\pi$ and $S\gamma$, depending upon a window in $M_{\pi\gamma}$. This analysis has shown that a reasonable $\sqrt{s}$ dependence of the cross section for the two processes is found in data. However, in doing this event by event separation, we have excluded any possible interference between these two production

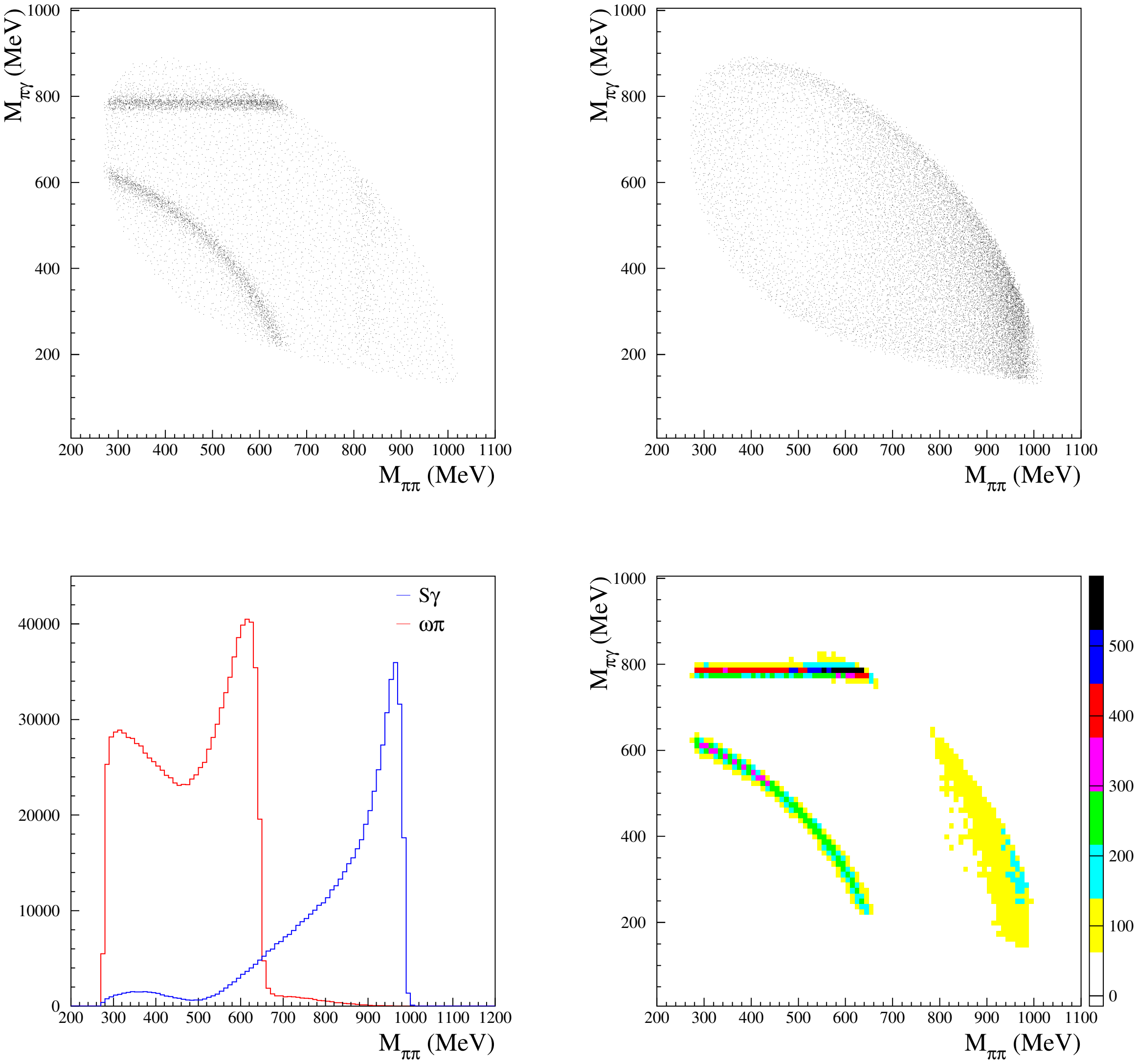

Figure 1: Dalitz plot for Montecarlo $\omega\pi$ (top-left) and $S\gamma$ (top-right) events. The MC expected relative size of the two contributions is shown as a function of $M_{\pi\pi}$ in the bottom-left panel. Dalitz plot for data collected at $\sqrt{s} = 1019.75$ (bottom-right) clearly shows the presence of both $S\gamma$ and $\omega\pi$ processes.

mechanisms, which is surely a first order approximation.

3. **Fit to the Dalitz plot and VMD-$S\gamma$ interference**
   In order to study the interference between the $\omega\pi$ and $S\gamma$ channels we do not divide them in categories and we just fit the whole Dalitz plot plane by folding the theory functions with the expected resolution and efficiencies. In the theory functions, the interference is properly taken into account although we expect the contribution to be small and almost negligible in the $M_{\pi\pi}$ region above 700 MeV.

The analysis shown in this note addresses most of the problems and comments related to our measurement which concerned either the $\omega\pi$ background subtraction or the small errors assigned to the $d\Gamma/dM_{\pi\pi}$ in the dip region observed at $M_{\pi\pi} \approx 500$ MeV due to the used unfolding procedure [4]. As mentioned in point 3, we now avoid these problems by not subtracting any VMD process and by just extracting parameters from the fit, obtained by folding theory models with our experimental effects. The only disadvantage of this approach is that we cannot provide to theorists our data in a simple way for fitting.

The organization of this note is the following: in Sec. 2 we recall the data sample used and the estimate of the background and efficiency, in Sec. 3 the different theory models are described and in Sec. 4 the fit method is explained. Finally in Sec. 5 the fit results are presented for the $\sqrt{s}$ value with higher statistics (1019.75 MeV) and then extrapolated to other close $\sqrt{s}$ points. Moreover we compare our results with KLOE latest published work on $\pi^+\pi^-\gamma$ [1].

2 Data sample, background and efficiency

In this section, we summarize the analysis performed on the data sample and the estimate of the residual background and signal efficiency. A much more detailed description of these items can be found in Ref. [4].

All 2001-2002 data were divided in $\sqrt{s}$ bin of 100 keV. For fitting purposes, we use only the highest statistical sample in the $\sqrt{s}$ bin closer to M_ϕ. This corresponds to 145 pb^{-1} collected at $\sqrt{s} = 1019.75$ MeV, where the beam energy scale has been corrected by fitting the resonance curve of $\phi \to \eta\gamma \to 3\pi^0\gamma$ events. The other four closest beam energy points are used to test the stability of the fit around M_ϕ. The data reduction consists of four steps: (i) an acceptance requirement of five prompt photons, (ii) a kinematic fitting imposing the ϕ 4-momentum to these photons, (iii) a process independent pairing procedure of photons to π^0's and (iv) a second kinematic fit where also the constraints on the π^0 masses are imposed. For the selected beam energy, after point (i) we start with a sample of 243,904 events of which 86,449 survive the complete analysis chain.

We recall that the two kinematic variables chosen for the construction of the Dalitz plot are the invariant masses of the two π^0's, $M_{\pi\pi}$, and of the two possible $\pi^0\gamma$ combinations, $M_{\pi\gamma}$. In the Dalitz plot we have therefore two entries per event. The binning choice, driven by the mass resolutions obtained by Montecarlo for the signal, is 10 MeV for $M_{\pi\pi}$ and 12.5 MeV for $M_{\pi\gamma}$. In Fig. 2 the difference between the reconstructed and the generated mass for both kinematic variables is shown. The distributions are fit with two Gaussian plus a constant contribution due to events where photons are not correctly paired to π^0's. The selected bin size is around three times the width of the narrower Gaussian and of the same order of the width of the second one.

The effect of the $\chi^2_{\rm Fit2}$ cut on signal efficiency and background rejection has been explained in detail in Ref. [4]. Here we just recall that a tighter cut has a better background rejection but creates a mass dependence of the efficiency for the VMD processes. In Figs. 3, 4 the distribution of the efficiency as a function of the two independent Dalitz plot variables is reported for both $\omega\pi$ and $S\gamma$ events. The different colours corresponds to different cuts on $\chi^2_{\rm Fit2}$. We fit the Dalitz plot for the case $\chi^2_{\rm Fit}/{\rm N_{dof}} < 5$ while the $\chi^2_{\rm Fit}/{\rm N_{dof}} < 3$ cut is used to test the systematics connected to the evaluation of the efficiency and to the background subtraction.

In Fig. 5, the different Dalitz plots refer to the main backgrounds with final states

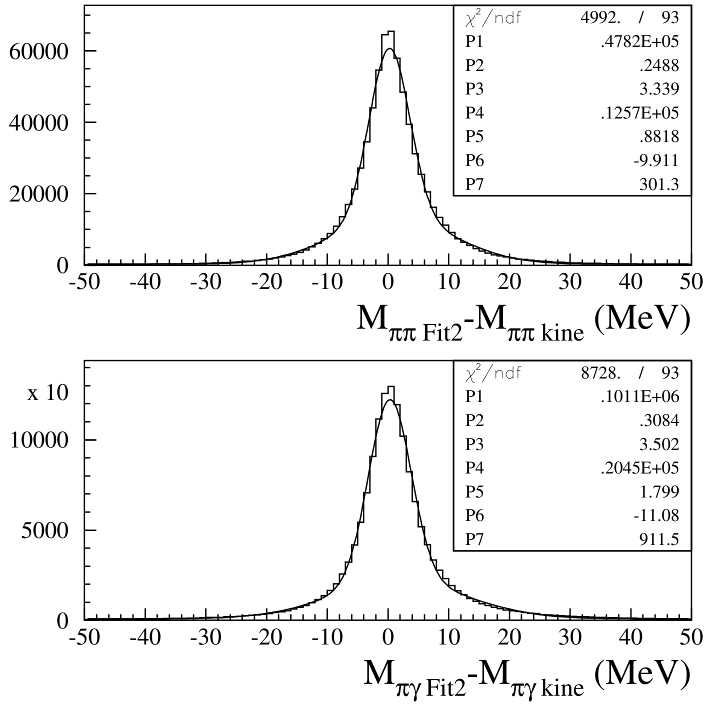

Figure 2: Mass resolution for $\pi^0\pi^0$ (top) and $\pi^0\gamma$ (bottom) invariant mass distributions: the mass is reconstructed using the output of the kinematic fit after the photon pairing. The resolution is estimated by subtracting the mass obtained by the Montecarlo generated momenta.

different from $\pi^0\pi^0\gamma$. The largest contribution is due to $\phi \to \eta\gamma \to \pi^0\pi^0\pi^0\gamma$ where the signal over background ratio is S/B $\approx$ 4. There are also contributions from $\phi \to \eta\pi^0\gamma$ (S/B $\approx$ 20) and events with three photons in the final states, with S/B $\approx$ 30. The calibration of the different backgrounds in the data sample has been performed by fitting background enriched data samples with the expected MC shapes. The resulting scale factors are close to 1 for the most relevant background channels and are not applied; we only use them in the evaluation of the systematic error as described in Ref. [4].

The data density is shown in Figs. 6.top before and after background subtraction. In the latter plot the Dalitz plot regions dominated by background are nicely uniform. The

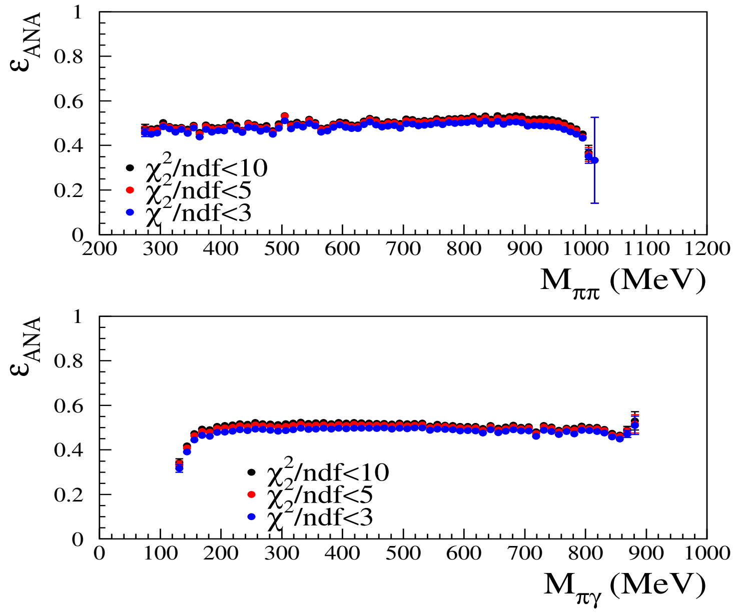

Figure 3: Analysis efficiency for $S\gamma$ MC events as a function of $M_{\pi\pi}$ and $M_{\pi\gamma}$.

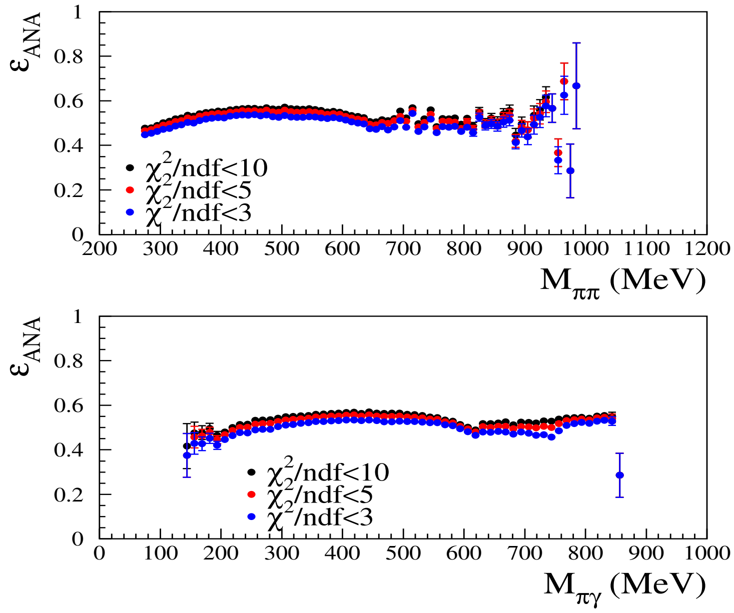

Figure 4: Analysis efficiency for $\omega\pi$ MC events as a function of $M_{\pi\pi}$ and $M_{\pi\gamma}$.

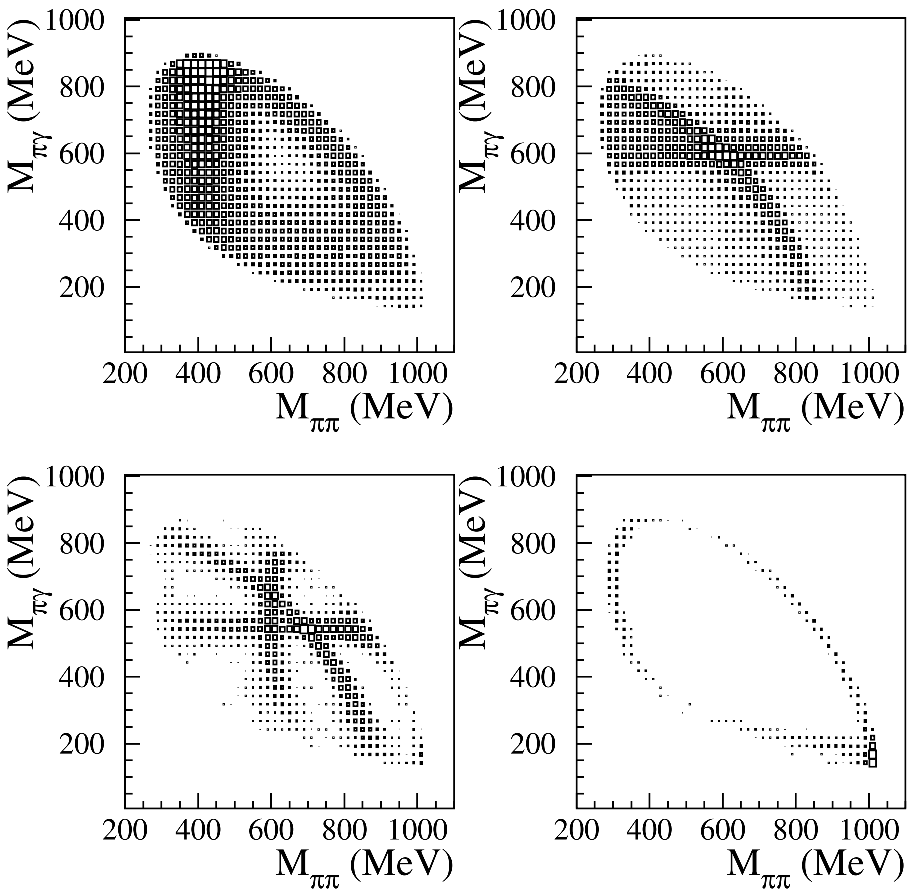

Figure 5: Dalitz plot for simulated background events: $\phi \to \eta\gamma \to \pi^0\pi^0\pi^0\gamma$ (top-left), $\phi \to \eta\pi^0\gamma \to \gamma\gamma\pi^0\gamma$ (top-right), $\phi \to \eta\gamma \to \gamma\gamma\gamma$ (bottom-left) and $\phi \to \pi^0\gamma$ (bottom-right).

projections of the Dalitz plot are instead shown in Figs. 6.bottom. A clean ω peak is visible in the $M_{\pi\gamma}$ distribution while in the $M_{\pi\pi}$ variable a small peak appears around 800 MeV due to the wrong pairing of photons to π^0's for $\omega\pi$ events. After background subtraction the number of events in the Dalitz plot is $128,529 \pm 659$.

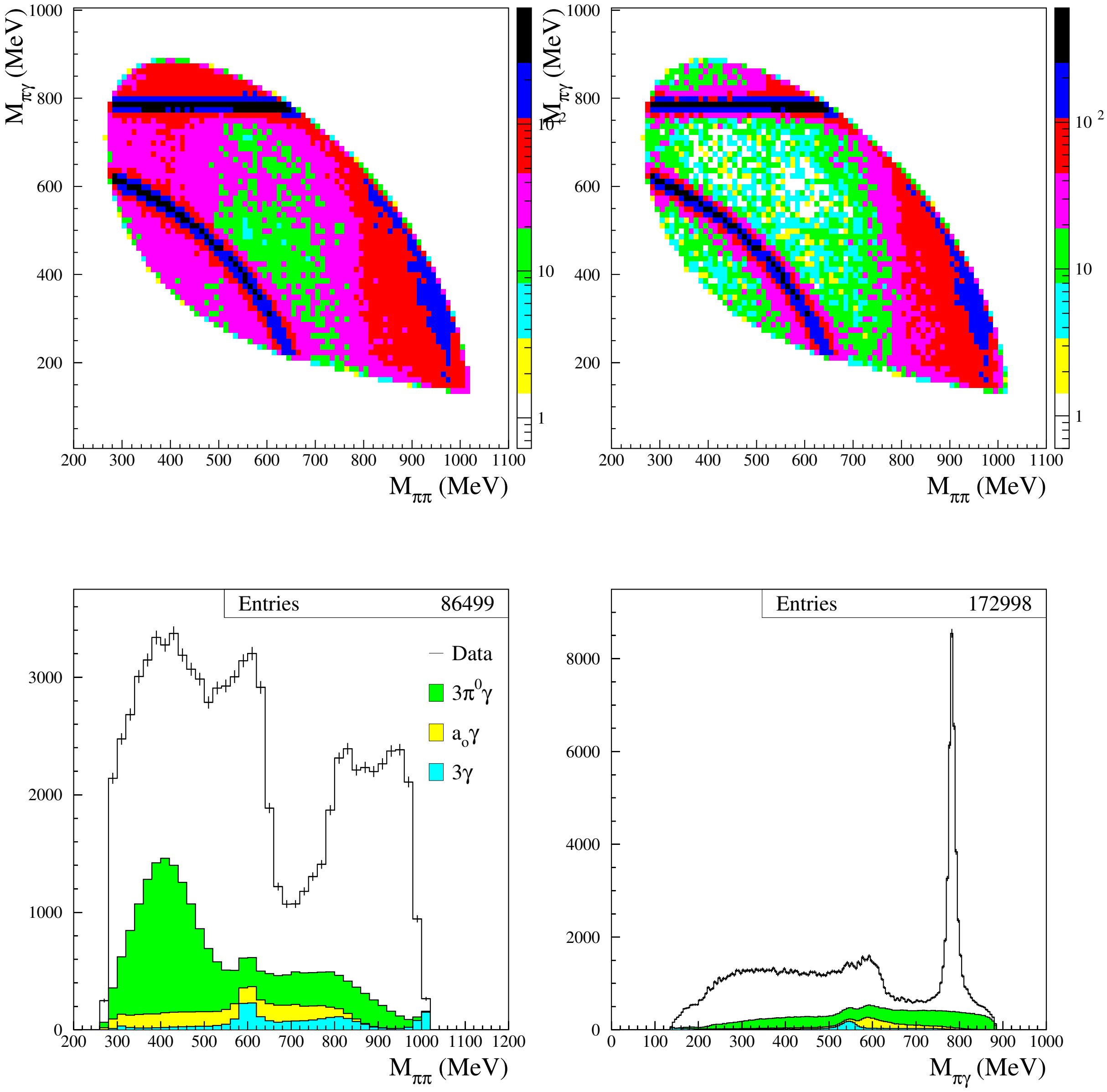

Figure 6: Top: Dalitz plot for data before (left) and after (right) background subtraction. To better appreciate the contributions from the background, logarithmic scale is used for the colour chart. Bottom: $M_{\pi\gamma}$ and $M_{\pi\pi}$ distributions before background subtraction.

3 Theoretical description of the process

At center of mass energy around M_ϕ, the $\pi^0\pi^0\gamma$ final state is dominated by the resonant process $\phi \to S\gamma \to \pi^0\pi^0\gamma$ ($S\gamma$), with a scalar meson in the intermediate state, and by the not resonant contribution $e^+e^- \to \pi^0\pi^0\gamma$ ($\omega\pi$). The amplitude of the $S\gamma$ process, M_S, will be described in the next subsections for the different models considered. The $\omega\pi$ is instead fully described by the Vector Meson Dominance model (VMD) and a complete formulation of the cross section can be found in literature [5, 6, 7]. The most general amplitude for the VMD term is given by

$$M_{V_1,V_2} = e^{i\delta_{b_{V_2}}}\, g_{V_1V_2\pi^0}\, g_{V_2\pi^0\gamma}\, V_{1,\alpha}\, p_\nu\, \epsilon_\delta\, q_\epsilon\, \epsilon_{\alpha\beta\mu\nu}\, \epsilon_{\beta\delta\omega\epsilon} \left(\frac{k_{1\mu}k_{2\omega}}{D_{V_2}(q+k_2)} + \frac{k_{2\mu}k_{1\omega}}{D_{V_2}(q+k_1)} \right) \quad (1)$$

where V_1 and V_2 are the vector mesons involved in production and decay: $V_1(p) \to V_2\pi^0 \to \gamma(q)\pi^0(k_1)\pi^0(k_2)$. Any light vector meson can contribute to this process to some extent: ρ, ω, ϕ, ρ', ρ'', ω', ω''... The largest cross-section is due to the ρ-ω pair trough the intermediate state $\rho \to \omega\pi^0$. Following the literature, it is also possible to introduce a term related to the phase of the decay vector, $e^{i\delta_{b_{V_2}}}$, in the amplitude [8]. There are theoretical arguments suggesting that the phase δ_{b_ω} should be small while δ_{b_ρ} can give a large contribution due to $\rho\pi^0$ rescattering. We have then include it in the VMD description.

The double differential $\pi^0\pi^0\gamma$ cross section can therefore be written as the sum of three terms: $S\gamma$, $\omega\pi$ and their relative interference [8]:

$$\begin{aligned} \frac{d\sigma}{dM_{\pi\pi}dM_{\pi\gamma}} \quad = \quad & \frac{\alpha\, M_{\pi\gamma}M_{\pi\pi}}{3(4\pi)^2 s^3} \left\{ \frac{g_{\phi\gamma}}{|D_\phi(s)|^2}|M_S|^2 + \frac{1}{16}F_1(M^2_{\pi\pi}, M^2_{\pi\gamma})|G_{\rho,\omega}(s, M^2_{\pi\gamma})|^2 + \right. \\ & \frac{1}{16}F_1(M^2_{\pi\pi}, \tilde{M}^2_{\pi\gamma})|G_{\rho,\omega}(s, \tilde{M}^2_{\pi\gamma})|^2 + \\ & \frac{1}{8}F_2(M^2_{\pi\pi}, M^2_{\pi\gamma})\, \Re e\, [G_{\rho,\omega}(s, M^2_{\pi\gamma})G^*_{\rho,\omega}(s, \tilde{M}^2_{\pi\gamma})] \pm \\ & \frac{1}{\sqrt{2}}\, \Re e \left[\frac{g_{\phi\gamma}}{D_\phi(s)} M_{S\gamma}[F_3(M^2_{\pi\pi}, M^2_{\pi\gamma})G^*_{\rho,\omega}(s, M^2_{\pi\gamma}) + \right. \\ & \left.\left. F_3(M^2_{\pi\pi}, \tilde{M}^2_{\pi\gamma})G^*_{\rho,\omega}(s, \tilde{M}^2_{\pi\gamma})] \right] \end{aligned} \quad (2)$$

The VMD contribution is made of three terms due to the exchange of identical pions ($M_{\pi\gamma}$ *vs* $\tilde{M}_{\pi\gamma}$) and their interference term. The full expression of the three coefficients $F_i(M^2_{\pi\pi}, M^2_{\pi\gamma})$, can be found in App. A while $G_{\rho,\omega}(s, M^2_{\pi\gamma})$ is simply given by the sum of many Breit-Wigner's as follows:

$$G_{\rho,\omega}(s, M_{\pi\gamma}^2) = \frac{e^{i\delta_{b_\rho}} A_{\rho\pi}(s)\, g_{\rho\pi\gamma}}{D_\rho(M_{\pi\gamma}^2)} + \frac{A_{\omega\pi}(s)\, g_{\omega\pi\gamma}}{D_\omega(M_{\pi\gamma}^2)} \tag{3}$$

The single amplitudes $A_{V\pi}(s)$ are expressed as:

$$A_{\rho\pi}(s) \;=\; \sum_{V=\phi,\omega,\omega',\omega''} \frac{g_{V\gamma}\, g_{V\rho\pi}}{D_V(s)}\, e^{i\phi_{\omega V(s)}} \tag{4}$$

$$A_{\omega\pi}(s) \;=\; \sum_{V=\rho,\rho',\rho''} \frac{g_{V\gamma}\, g_{V\omega\pi}}{D_V(s)}\, e^{i\phi_{\rho V(s)}} \tag{5}$$

where the $g_{V\gamma}$ constants are related to the mass and width of the vector meson as follows: $g_{V\gamma} = \sqrt{3M_V^3 \Gamma_V B(V \to e^+e^-)/\alpha}$. For $s \sim M_\phi^2$, the uncertainty arising from the mesons ω', ω'', ρ' and ρ'' can be avoided by fitting some complex constants $C_{\omega\pi} = g_{\omega\pi\gamma} A_{\omega\pi}(M_\phi^2)$, $C_{\rho\pi} = g_{\rho\pi\gamma} \overline{A}_{\rho\pi}(M_\phi^2)$, where $\overline{A}_{\rho\pi}$ is the not resonant amplitude which does not contain the ϕ contribution. With this transformation the $G_{\rho,\omega}$ terms become:

$$G_{\rho\pi}(s, M_{\pi\gamma}^2) \;=\; \left(\frac{e^{i\phi_{\omega\phi}(M_\phi^2)}\, g_{\phi\gamma}\, g_{\phi\rho\pi}\, g_{\rho\pi\gamma}}{D_\phi(s)} + C_{\rho\pi} \right) \frac{e^{i\delta_{b_\rho}}}{D_\rho(M_{\pi\gamma}^2)} \tag{6}$$

$$G_{\omega\pi}(s, M_{\pi\gamma}^2) \;=\; \frac{C_{\omega\pi}}{D_\omega(M_{\pi\gamma}^2)} \tag{7}$$

As a starting point of our fit we use the parameters calculated at M_ϕ by N. N. Achasov [8] using Tab. V of [9]:

$$C_{\rho\pi} \;\sim\; (-0.45 \pm 0.16\, i\,)\ \text{GeV}^{-1} \times g_{\rho\pi\gamma} \sim (-0.12 \pm 0.04\, i\,)\ \text{GeV}^{-2} \tag{8}$$

$$C_{\omega\pi} \;\sim\; (-1.2 \;\; \pm 0.6 \;\; i\,)\ \text{GeV}^{-1} \times g_{\omega\pi\gamma} \sim (\;\; 0.9 \;\; \pm 0.4 \;\; i\,)\ \text{GeV}^{-2} \tag{9}$$

These numbers have a 20% precision on $|C_{V\pi}|$ and the phases are not precisely measured.

To give a flavour of the way in which the VMD cross section looks like, we have plotted in Fig. 7 the $M_{\pi\pi}$ projection of the Dalitz plot for the different contributions. The $\omega\pi$ term is dominant and the introduction of δ_{b_ρ} modifies the $M_{\pi\pi}$ shape.

Concerning the scalar term, we use two different approaches for the description of the amplitude: the Kaon Loop model [10, 11] (KL), where the scalar is coupled to the ϕ through a charged kaon loop, and the so called "No Structure" model [12] (NS). Here the $\phi f_0 \gamma$ coupling is point-like and the scalar is described as a Breit-Wigner with a mass dependent width added to a polynomial complex function to allow an appropriate dumping of the resulting shape. The Scattering Amplitude approach [13] has not been used since it does not provide a good description of the $\pi^+\pi^-\gamma$ final state.

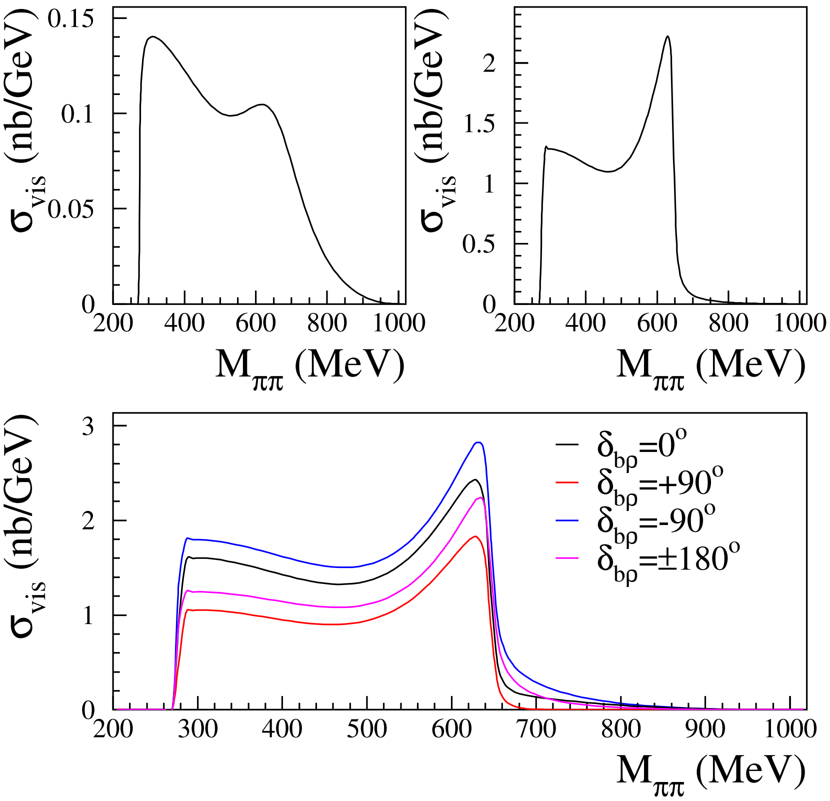

Figure 7: Vector Meson Dominance contributions to the $\pi^0\pi^0\gamma$ final state as a function of $M_{\pi\pi}$: $V \to \rho\pi$ (up.left), $V \to \omega\pi$ (up.right) and the sum of the two for different values of the δ_{b_ρ} phase.

3.1 Kaon Loop Model

As scalar term for the kaon loop model we use the one described in the latest published paper by N. N. Achasov [14]. In this version, the amplitude of the signal $\phi \to S\gamma \to \pi^0\pi^0\gamma$ takes into account the mixing of two scalar states S and S', namely the $f_0(980)$ and the $\sigma(600)$, and well reproduces our old published data in the 1-dimensional analysis [2]. The amplitude is similar to the one reported in Ref. [15] for the analysis of $f_0(980) \to \pi^+\pi^-$, where:

$$M_S = e^{i\delta_B} g(M_{\pi\pi}) \left(\sum_{S,S'} g_{SK^+K^-}\, G^{-1}_{SS'}\, g_{S'\pi^0\pi^0} \right) , \tag{10}$$

the only difference being the description of the δ_B phase. In this expression, the $g(M_{\pi\pi})$ is the kaon loop function defined in Ref. [10], which acts as a sort of effective form factor and reduces the E_γ^3 divergency in the $M_{\pi\pi}$ mass spectrum obtained when assuming a point-like coupling between the scalar and the ϕ meson. The propagator matrix $G_{SS'}$ is instead given by:

$$G_{SS'}(M_{\pi\pi}) = \begin{pmatrix} D_S(M_{\pi\pi}) & -\Pi_{SS'}(M_{\pi\pi}) \\ -\Pi_{S'S}(M_{\pi\pi}) & D_{S'}(M_{\pi\pi}) \end{pmatrix} \tag{11}$$

where D_S is the inverse propagator of the scalar, which is written as:

$$D_S(M_{\pi\pi}) = M_S^2 - M_{\pi\pi} + \sum_{ab} g_{Sab} \left\{ \Re[P_S^{ab}(M_S^2)] - P_S^{ab}(M_{\pi\pi}) \right\} \tag{12}$$

The last term, explicitly reported in Ref. [10], is a sum extended over all the possible two particle decay products of the scalar.[1] It takes into account the finite width correction of the resonance and reproduces the threshold effect. The non-diagonal term $\Pi_{SS'}$ express the probability of mixing between the two scalar mesons:

$$\Pi_{SS'}(M_{\pi\pi}) = \sum_{ab} g_{S'ab} P_S^{ab}(M_{\pi\pi}) + C_{SS'} , \tag{13}$$

where the $C_{SS'}$ takes into account the contribution from intermediate state other than ab. Finally, $g_{SK^+K^-}$, $g_{S\pi^0\pi^0}$ are the coupling constants of the scalar to the K^+K^- and $\pi^0\pi^0$ final states, and are related to the width of the scalar meson as follows:

$$\Gamma(S \to ab\,; M_{\pi\pi}) = \frac{g_{Sab}^2}{16\pi M_{\pi\pi}} \rho_{ab}(M_{\pi\pi}) , \tag{14}$$

[1] We have taken into account in the inverse propagator the following final states: $\pi^+\pi^-$, $\pi^0\pi^0$, K^+K^-, $K^0\bar{K}^0$, $\eta\eta$, $\eta\eta'$ and $\eta'\eta'$.

where $\rho_{ab}(M_{\pi\pi}) = \sqrt{(M_{\pi\pi}^2 - M_+^2)(M_{\pi\pi}^2 - M_-^2)}/M_{\pi\pi}^2$ and $M_\pm = M_a \pm M_b$.

In the old KL model the phase δ_B takes into account only the elastic background scattering due to $\pi\pi$.[2] In the new formulation also the elastic scattering due to $K\overline{K}$ is considered. For this reason the phase δ_B is now expressed as the sum of two contributions:

$$\delta_B = \delta_B^{\pi\pi} + \delta_B^{KK}. \tag{15}$$

The two phases are parametrized as follows, taking into account that, in the case of a light σ, the expression for $\delta_B^{\pi\pi}$ should provide chiral shielding of σ [16]:

$$\tan\delta_B^{\pi\pi} = -\frac{p_\pi}{2\,M_\pi}\left(b_0 - b_1\frac{p_\pi^2}{(2\,M_\pi)^2} + b_2\frac{p_\pi^4}{(2\,M_\pi)^4}\right)\frac{1}{1+p_\pi^2/\Lambda^2} \tag{16}$$

$$\tan\delta_B^{KK} = f_K(M_{\pi\pi}^2)\sqrt{M_{\pi\pi}^2 - 4\,M_{K^+}^2} \tag{17}$$

In these expressions $p_\pi = \sqrt{M_{\pi\pi}^2 - 4M_\pi^2}$ and $f_K(M_{\pi\pi}^2) = -\arctan\frac{M_{\pi\pi}^2 - m_1^2}{m_2^2}/\Lambda_K$. Due to the analytical continuation of $e^{i\delta_B^{KK}}$, below the $K\overline{K}$ threshold the additional phase changes the amplitude M_S of a factor:

$$P_K = \sqrt{\frac{1 - f_K(M_{\pi\pi}^2)\sqrt{4\,M_{K^+}^2 - M_{\pi\pi}^2}}{1 + f_K(M_{\pi\pi}^2)\sqrt{4\,M_{K^+}^2 - M_{\pi\pi}^2}}}. \tag{18}$$

The theoretical advantage of this formulation is that it is simple to relate the $G_{SS'}$ matrix to the S-wave amplitude of the $\pi\pi$ scattering, T_0^0, and the inelasticity η_0^0:

$$T_0^0 = \frac{\eta_0^0\, e^{2i\delta_0^0 - 1} - 1}{2i\rho_{\pi\pi}(M_{\pi\pi})} = \frac{e^{2i\delta_B^{\pi\pi}} - 1}{2i\rho_{\pi\pi}(M_{\pi\pi})} + e^{2i\delta_B^{\pi\pi}}\sum_{SS'}\frac{g_{S\pi\pi}G_{SS'}^{-1}g_{S'\pi\pi}}{16\pi} \tag{19}$$

The phase δ_0^0 and the inelasticity have the form:

$$\delta_0^0(M_{\pi\pi}) = \delta_B^{\pi\pi}(M_{\pi\pi}) + \delta_{\rm res}(M_{\pi\pi}) \tag{20}$$

$$\eta_0^0(M_{\pi\pi}) = \begin{cases} 1 & M_{\pi\pi} \le 2M_{K^+} \\ |S^0_{0\,\rm res}| & M_{\pi\pi} > 2M_{K^+} \end{cases} \tag{21}$$

where $\delta_{\rm res}(M_{\pi\pi})$ is half of the phase of $S^0_{0\,\rm res}$, whose expression is

$$S^0_{0\,\rm res} = 1 + 2i\rho_{\pi\pi}(M_{\pi\pi})\sum_{SS'}\frac{g_{S\pi\pi}G_{SS'}^{-1}g_{S'\pi\pi}}{16\pi}. \tag{22}$$

[2] In the paper on the search of the $f_0(980) \to \pi^+\pi^-$ decay with 2001-2002 data [1] only this contribution has been taken into account.

Using this theoretical framework, our $\pi^0\pi^0$ mass spectrum obtained from 2000 data [2] has been fit together with $\pi\pi$ scattering data [17, 18, 19, 20, 21]. The two considered scalar states are the $f_0(980)$ and the $\sigma(600)$. The free parameters are the ones describing $\delta_B(M_{\pi\pi})$ (b_0, b_1, b_2 ,λ, m_0, m_2 ,λ_K) and the mass and the couplings of the scalars involved in the process: M_{f_0}, M_σ, $g_{f_0\pi^+\pi^-}$, $g_{f_0K^+K^-}$, $g_{\sigma\pi^+\pi^-}$, $g_{\sigma K^+K^-}$ and $C_{f_0\sigma}$. The connections between the coupling of the scalar with charged and neutral final states are: $g_{S\pi^+\pi^-} = \sqrt{2}g_{S\pi^0\pi^0}$ and $g_{SK^+K^-} = g_{SK^0\bar{K}^0}$. All the other couplings involved in the inverse propagators are fixed to the predictions of the 4-quark model:

$$g_{f_0\eta\eta} = -g_{f_0\eta'\eta'} = \frac{2\sqrt{2}}{3}g_{f_0K^+K^-} \tag{23}$$

$$g_{f_0\eta\eta'} = -\frac{\sqrt{2}}{3}g_{f_0K^+K^-} \tag{24}$$

$$g_{\sigma\eta\eta} = g_{\sigma\eta\eta'} = \frac{\sqrt{2}}{3}g_{\sigma\pi^+\pi^-} \tag{25}$$

$$g_{\sigma\eta'\eta'} = \frac{1}{3\sqrt{2}}g_{\sigma\pi^+\pi^-} \tag{26}$$

In order to follow some expected theoretical restrictions, the authors

1. remove singularities in the analytical continuation of the $\pi\pi \to K\overline{K}$ and $\pi\pi \to \pi\pi$ amplitudes;

2. fix the $\pi\pi$ scattering length to the calculation of Ref. [22] based on chiral perturbation theory and Roy equations;

3. set an Adler zero just below the $\pi\pi$ threshold to guarantee the weakness of $\pi\pi$ interactions near the threshold.

As can be seen in Ref. [14], the fit well reproduces the data points for both $M_{\pi\pi}$ and δ_0^0. Moreover, also the behaviour of η_0^0 is in good agreement with the theoretical expectation. There are ten different sets of parameters able to describe the experimental data. The χ^2 probability ranges between 47% and 79%.

3.2 No structure description

In this description [12], the amplitude of the scalar term, $A^{\rm scal}$, is proportional to a reduced scalar form factor, $F_0^{\rm scal}$, which is derived by assuming a direct coupling of the ϕ to the $f_0(980)$, $g_{\phi f_0 \gamma}$, and a subsequent coupling of the f_0 to the $\pi\pi$ pair, $g_{f_0\pi\pi}$. In the same form factor the possible not-resonant continuum background is also added as a series expansion in $M_{\pi\pi}$ as follows:

$$F_0^{\rm scal} = \frac{g_{f_0\pi\pi}\, g_{\phi f_0 \gamma}}{M_{\pi\pi}^2 - M_{f_0}^2 + i\, M_{\pi\pi}\Gamma_{f_0}(M_{\pi\pi})} + \frac{a_0}{M_\phi^2} e^{ib_0 \frac{v_\pi(M_{\pi\pi})}{M_\phi}} + \frac{a_1}{M_\phi^4} e^{ib_1 \frac{v_\pi(M_{\pi\pi})}{M_\phi}} (M_{\pi\pi}^2 - M_{f_0}^2), \quad (27)$$

where, in the most general case, the background parameters are complex numbers and $v_\pi(M_{\pi\pi})$ is proportional to pion momentum in the f_0 rest frame, $v_\pi = \sqrt{M_{\pi\pi}^2/4 - M_\pi^2}$. The propagator for the narrow resonance is described by a simple Breit-Wigner shape corrected by the Flattè condition on the $\pi\pi$ and KK thresholds, i.e.:

$$\Gamma_{f_0}(M_{\pi\pi}) = g_{f_0\pi\pi}^2 \frac{v_\pi(M_{\pi\pi})}{8\pi M_{\pi\pi}^2} + g_{f_0 KK}^2 \frac{v_K(M_{\pi\pi}) + v_{K^0}(M_{\pi\pi})}{8\pi M_{\pi\pi}^2}, \quad (28)$$

where the velocities v_{π,K,K^0} are complex numbers with an analytical continuation under threshold. Just to be complete, we recall that the relation between the coupling constants and the f_0 width in the neutral final state is given by:

$$\Gamma(f_0 \to \pi\pi\, ;\, M_{\pi\pi}) = \frac{g_{f_0\pi\pi}^2}{16\pi M_{\pi\pi}} \sqrt{1 - 4M_\pi^2/M_{\pi\pi}^2}\,, \quad (29)$$

in agreement with KL definition.

In order to reduce the number of free parameters, a constraint on the phases of the scalar form factor, $\phi_s = \arctan(\Im(F_0^{scal})/\Re(F_0^{scal}))$, is imposed by requiring that, close to threshold, this phase should coincide with the $\pi\pi$ S-wave elastic phase, δ_0^0. With this requirement, the b_0 phase in Eq. (27) is fully determined as a function of the other parameters. The number of free parameters is then seven: the f_0 mass and three related coupling constants ($g_{\phi f_0\gamma}$, $g_{f_0\pi\pi}$ and g_{f_0KK}) plus a_0, a_1 and b_1 for the background. We refer to this description as N_1 in the following.

A light $\sigma(600)$ meson can be added in this framework by reducing at the same time the number of free parameters for the continuum background. The idea is to use a BW for a broad resonance while dropping instead the quadratic term of Eq. (27):

$$F_0^{\rm scal} = \frac{g_{f_0\pi\pi}\, g_{\phi f_0 \gamma}}{M_{\pi\pi}^2 - M_{f_0}^2 + i\, M_{\pi\pi}\Gamma_{f_0}(M_{\pi\pi})} + \frac{a_0}{M_\phi^2} e^{ib_0 \frac{v_\pi(M_{\pi\pi})}{M_\phi}} + \frac{g_{\sigma\pi\pi}\, g_{\phi\sigma\gamma}}{M_{\pi\pi}^2 - M_\sigma^2 + i\, M_{\pi\pi}\Gamma_\sigma(M_{\pi\pi})}, \quad (30)$$

where $g_{\phi\sigma\gamma}$ represents the $\sigma(600)$ coupling to the ϕ meson. In the used approximation, called N2, the $\sigma(600)$ width is assumed to be dominated by couplings to the pions as:

$$\Gamma_\sigma(M_{\pi\pi}) = g^2_{\sigma\pi\pi}\frac{v_\pi(M_{\pi\pi})}{8\pi M_{\pi\pi}}, \tag{31}$$

and the value of the coupling constant is obtained by constraining it to the experimental mass and width[3] coming from Ref. [23]. Also in this case, the requirement of fixing the scalar form factor phase close to threshold to δ^0_0 allows the b_0 phase to be completely determined as a function of the other parameters. On doing so, we remain with six free parameters: the f_0 mass and its three couplings, a_0 for the continuum background and the coupling of the $\sigma(600)$ meson to the ϕ.

4 Fit method

The Dalitz plot data density is shown in Fig. 6.top before and after background subtraction. For each i^{th} bin of the Dalitz plot, the number of events is defined as N_i, the expected background B_i and the final signal counting is $S_i = N_i - B_i$, with a corresponding error of $\delta S_i = \sqrt{N_i + B_i}$. In quadrature to this error we also add the systematic error due to the background knowledge.

When fitting data we use the two different theories described before by performing a convolution with the experimental effects. The expected number of events for a given $M_{\pi\pi}$, $M_{\pi\gamma}$ bin i, N_i^{exp}, is obtained as the sum of the contributions from all theoretical bins j multiplied by the total integrated luminosity, $\mathcal{L}$ as follows:

$$N_i^{\text{exp}} = \mathcal{L} \times \sum_j (f_j^V \; A^V(i,j)\; \varepsilon_j^V + f_j^S \; A^S(i,j)\; \varepsilon_j^S + f_j^I \; A^V(i,j)\; \varepsilon_j^V). \tag{32}$$

In this formula, f_j is the integration of the differential cross section evaluated in the j^{th} bin.[4] The suffixes V and S stay for VMD and $S\gamma$ terms while I represents their interference. The correction for the average radiator function, $H^{V,S}(\sqrt{s})$, is also performed

[3]The value of M_σ and Γ_σ used are (526 ± 15) MeV and (535 ± 50) MeV respectively, which correspond to a value of $g_{\sigma\pi\pi}$ of 4.1$\pm$ 0.2 GeV.

[4]When we estimate the theory contribution for a given reconstructed bin of size $\Delta M_{\pi\pi} \times \Delta M_{\pi\gamma}$, we numerically integrate the theory event density by subdividing this bin in a 5×5 grid of theory points. In other words we count $\sum_{i,j}^{1,5} \frac{d\sigma(m_1^i, m_2^j)}{dm_1 dm_2} \times dm_1 dm_2$, where dm_1, dm_2 are $\Delta M_{\pi\pi}/5$ and $\Delta M_{\pi\gamma}/5$ respectively with $m_1^i = M_{\pi\pi}^{min} + dm_1 \times (i-1)$ and $m_2^j = M_{\pi\gamma}^{min} + dm_2 \times (j-1)$.

when evaluating f_i.[5] For each bin, ε_j is the analysis efficiency while $A(i,j)$ is the smearing matrix, representing the probability for the signal event to migrate from the $j^{\rm th}$ to the $i^{\rm th}$ bin either due to resolution or to a wrong reconstruction of the event. This matrix has been evaluated by Montecarlo. In Figs. 8, the behaviour of this smearing matrix is shown for both $S\gamma$ and $\omega\pi$ processes. The x-axis runs on the generated $M_{\pi\pi}$–$M_{\pi\gamma}$ mass bins of the Dalitz plot; the index number is obtained by slicing the Dalitz plot in $M_{\pi\pi}$ and running on $M_{\pi\gamma}$. Similarly, the y-axis runs on the reconstructed mass. The content of each bin is weighted by $A(i,j)$. Around 85% of the events are on the diagonal or close to it in within ± 1 bin (due to the large resolution tails). The different pattern of the smearing matrix between $S\gamma$ and $\omega\pi$ events is due to the different kinematics of the two processes. In order to measure from data the quantity of bad reconstructed events, mainly due to a wrong photon pairing into π^0's, we fit the difference of the two lowest χ^2 value used to combine photons [4]. We conclude that Montecarlo underestimates the quantity of wrong pairing of $(8.0 \pm 0.1)\%$. An independent check of the reasonable goodness of the smearing matrix is shown in Fig. 9 where the data-MC comparison for $\omega\pi$ events, selected with the exclusive analysis described in Ref. [24], is reported. As shown in Fig. 1, the VMD contribution is concentrated in the region $M_{\pi\pi} < 650$ MeV. Events with higher $M_{\pi\pi}$ values have a wrong photon pairing and thus belong to the not diagonal smearing matrix region. The data-MC agreement in this region is very good.

To estimate the theory parameters $p_1, p_2 \ldots p_n$ from the fit, we calculate the χ^2 as follows:

$$\chi^2 = \sum_i \left(N_i^{exp}(p_1, p_2 \ldots p_n) - S_i\right)^2 / \delta_S^2 \tag{33}$$

and we then minimize it. The minimization of this multi-parameters function is done using the MINUIT package [25]. Only the experimental bins inside the kinematical boundaries of the Dalitz plot are used to evaluate the χ^2.

[5] The average correction has been evaluated as a function of $\sqrt{s}$ using the formulae described in Ref. [4].

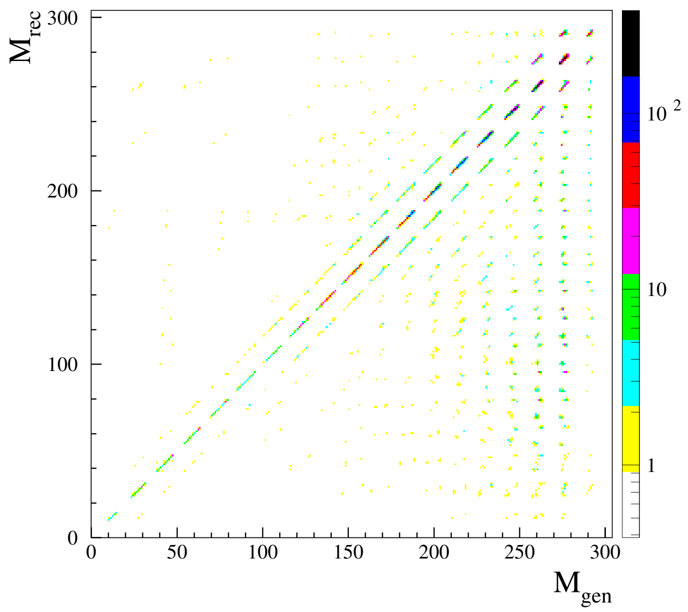

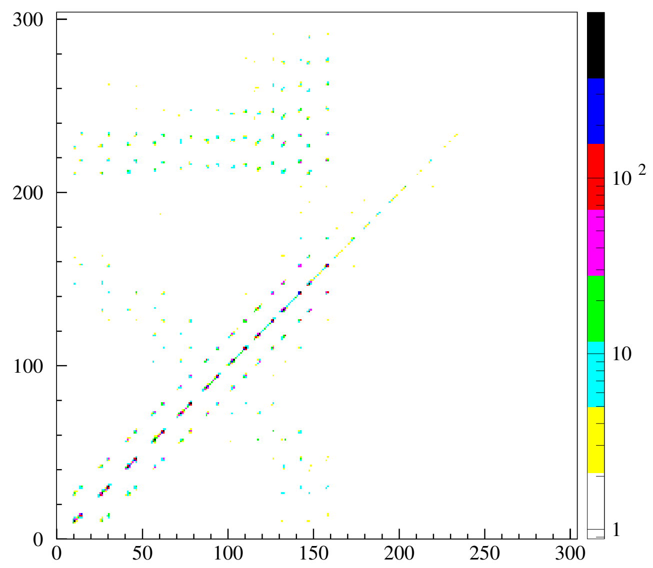

Figure 8: Smearing matrix for $S\gamma$ (top) and $\omega\pi$ (bottom) events.

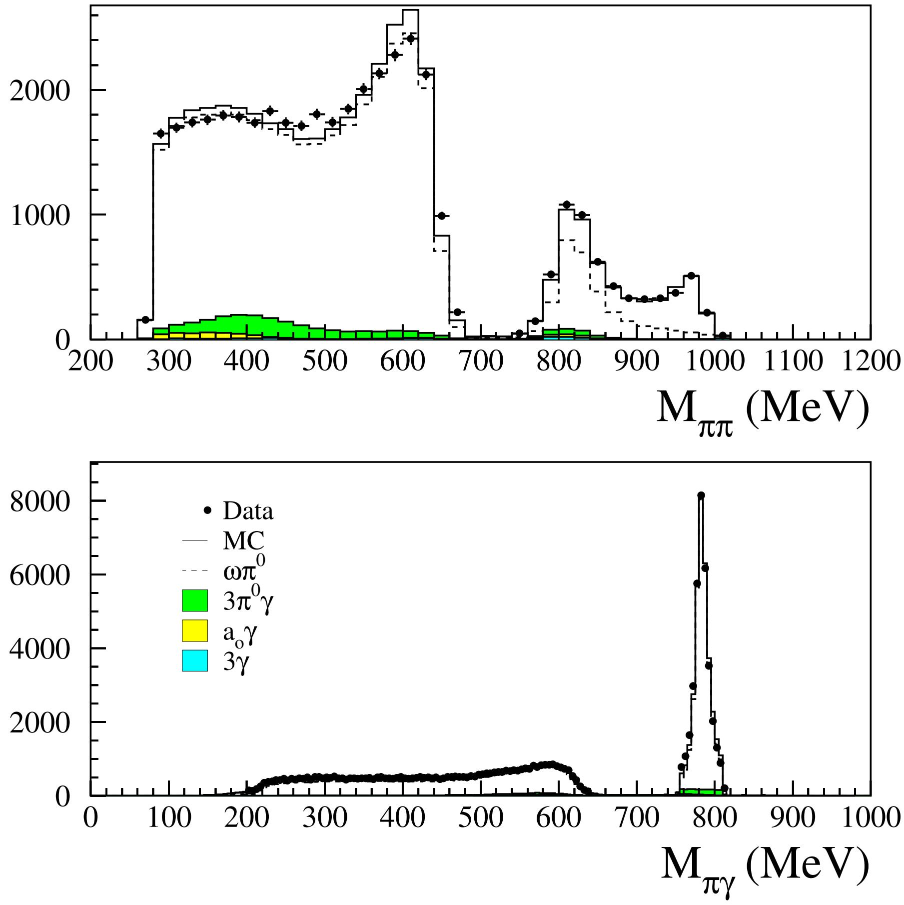

Figure 9: Projections of the Dalitz plot for $\omega\pi$ events selected with the exclusive analysis described in Ref. [4]. The small data-MC disagreement visible for $M_{\pi\pi} < 650$ MeV mostly reflects the neglection the of the $S\gamma$–$\omega\pi$ interference term.

5 Fit results

Since the theory formulation of the VMD background is appropriated only at $\sqrt{s} \sim M_\phi$, we fit only the highest statistical data sample close to the ϕ mass, 1019.75 MeV, corresponding to an integrated luminosity of 145 pb^{-1}. The center of mass energy scale has been corrected by 150 keV as shown in Ref. [4], following the calibration from the energy scan for $\phi \to \eta\gamma$ events, where we compare M_ϕ with the value reported in [26].

5.1 Fit results for the KL model

In the case of the kaon loop model, we can not leave all $f_0(980)$ and $\sigma(600)$ parameters free since the description of the elastic background, the position of the Adler zero and the couplings and masses of the $\sigma(600)$ meson are closely related. We therefore proceeded by leaving only the parameters describing the VMD and the $f_0(980)$ terms to vary freely. For the $\sigma(600)$ and the elastic parameters of $\pi\pi$ and $K\overline{K}$ scattering we used all the ten sets of parameters reported in Ref. [14], defined as K1, K2...K10. In general, the $\sigma(600)$ parameters satisfy the 4-quark model requirements: coupling to $K\overline{K}$ suppressed with respect to $\pi\pi$ and mass in the 500–700 MeV range, providing a very broad meson of width between 240 and 490 MeV. Moreover, the Adler zero is set just below the $\pi\pi$ threshold both for $T_0^0(\pi\pi \to \pi\pi)$ and $T_0^0(K\overline{K} \to \pi\pi)$. All the odd (even) variants have a positive (negative) $g_{\sigma\pi^+\pi^-}/g_{f_0K^+K^-}$ ratio. In more detail, in the first four data sets (K1 to K4) there is a small but not vanishing coupling between σ and K^+K^- ($g_{\sigma K^+K^-} = 0.55\,,\ -0.93\,,\ 0.43\,,\ -1.1$ GeV respectively). In K1, K2 and K3 the Adler zero in $K\overline{K} \to \pi\pi$ is set to M_π^2 while in K4 is set to $M_\pi^2/2$. K5 and K6 have instead the coupling values of the σ fixed to the naive 4-quark model i.e. $g_{\sigma K^+K^-}$ almost negligible (0.13 and -0.035 GeV respectively). In the last four data sets some of the general constraints are relaxed: in K7 and K8 the mass of the σ meson is around 400 MeV while in K9 and K10 the $K\overline{K} \to \pi\pi$ Adler zero is not bound in the $0 < M_{\pi\pi}^2 < 2\,M_\pi^2$ region, providing a zero around -1 GeV^2.

The fit results for the scalar parameters are reported in Tab. 1. When fixing the $\sigma(600)$ mass to the values of Ref. [14] we obtain $P(\chi^2)$ ranging from 10^{-5} to 15%. We consider acceptable just the six variants with $P(\chi^2) > 1\%$. For each parameter, we use the central value and the errors from the best fit as the result while we add an extra error associated to the theory model. This last error is the maximum variation between the central value

M_σ fixed

Fit	M_{f_0} (MeV)	$g_{f_0K^+K^-}$ (GeV)	$g_{f_0\pi^+\pi^-}$ (GeV)	M_σ, Γ_σ (MeV)	$\chi^2/\mathrm{N_{dof}}$	$P(\chi^2)$
K1	976.8 ± 0.3	3.76 ± 0.04	-1.43 ± 0.01	$462\,,286$	2754/2676	0.145
K2	986.2 ± 0.3	3.87 ± 0.08	-2.03 ± 0.02	$485\,,240$	2792/2676	0.058
K3	985.2 ± 0.2	4.92 ± 0.06	-1.92 ± 0.01	$472\,,320$	2809/2676	0.036
K4	987.3 ± 0.1	3.84 ± 0.11	-2.00 ± 0.02	$543\,,290$	2855/2676	0.008
K5	987.0 ± 0.2	2.61 ± 0.05	-0.95 ± 0.01	$709\,,493$	2970/2676	5×10^{-5}
K6	983.5 ± 0.4	2.52 ± 0.04	-0.82 ± 0.01	$693\,,442$	2981/2676	3×10^{-5}
K7	981.6 ± 0.2	4.53 ± 0.05	-1.90 ± 0.01	$400\,,242$	2852/2676	0.009
K8	982.3 ± 0.4	4.02 ± 0.06	-1.76 ± 0.02	$415\,,260$	2787/2676	0.066
K9	983.3 ± 0.2	3.75 ± 0.02	-1.40 ± 0.01	$529\,,366$	2823/2676	0.024
K10	986.9 ± 0.1	3.28 ± 0.05	-1.90 ± 0.01	$566\,,264$	2799/2676	0.048

M_σ free

Fit	M_{f_0} (MeV)	$g_{f_0K^+K^-}$ (GeV)	$g_{f_0\pi^+\pi^-}$ (GeV)	M_σ (MeV)	$\chi^2/\mathrm{N_{dof}}$	$P(\chi^2)$
K1	974.8 ± 0.6	3.49 ± 0.08	-1.29 ± 0.04	551 ± 15	2734/2675	0.208
K2	986.1 ± 0.2	3.75 ± 0.07	-1.99 ± 0.02	527 ± 13	2786/2675	0.066
K3	984.8 ± 0.4	4.65 ± 0.12	-1.81 ± 0.03	534 ± 13	2797/2675	0.049
K4	987.3 ± 0.1	4.06 ± 0.08	-2.07 ± 0.02	475 ± 25	2847/2675	0.010
K5	982.7 ± 0.4	2.42 ± 0.03	-0.95 ± 0.01	406 ± 15	2817/2675	0.027
K6	980.2 ± 0.4	2.45 ± 0.04	-0.89 ± 0.01	403 ± 61	2788/2675	0.062
K7	981.2 ± 0.5	4.41 ± 0.06	-1.82 ± 0.02	514 ± 18	2816/2675	0.028
K8	981.2 ± 0.3	3.73 ± 0.04	-1.64 ± 0.01	536 ± 10	2745/2675	0.168
K9	982.3 ± 0.3	3.49 ± 0.05	-1.29 ± 0.01	594 ± 6	2808/2675	0.036
K10	986.4 ± 0.5	2.95 ± 0.13	-1.80 ± 0.04	629 ± 17	2776/2675	0.085

Table 1: Fit results for the scalar term in the kaon loop model. Different rows are for the different sets of parameters used for the $\sigma(600)$ and the elastic parameters of $\pi\pi$ and $K\overline{K}$ scattering. Top table is when constraining the mass of the $\sigma(600)$ to the indicated value, bottom table is when leaving also the mass of the $\sigma(600)$ free to vary.

obtained by the best fit and all the other accepted fit variants. In order to test if we are sensitive to a change in the $\sigma(600)$ meson mass, we repeat all fits leaving M_σ free to vary. Results are summarized in Tab. 1.bottom. In all the cases the fit improves and M_σ

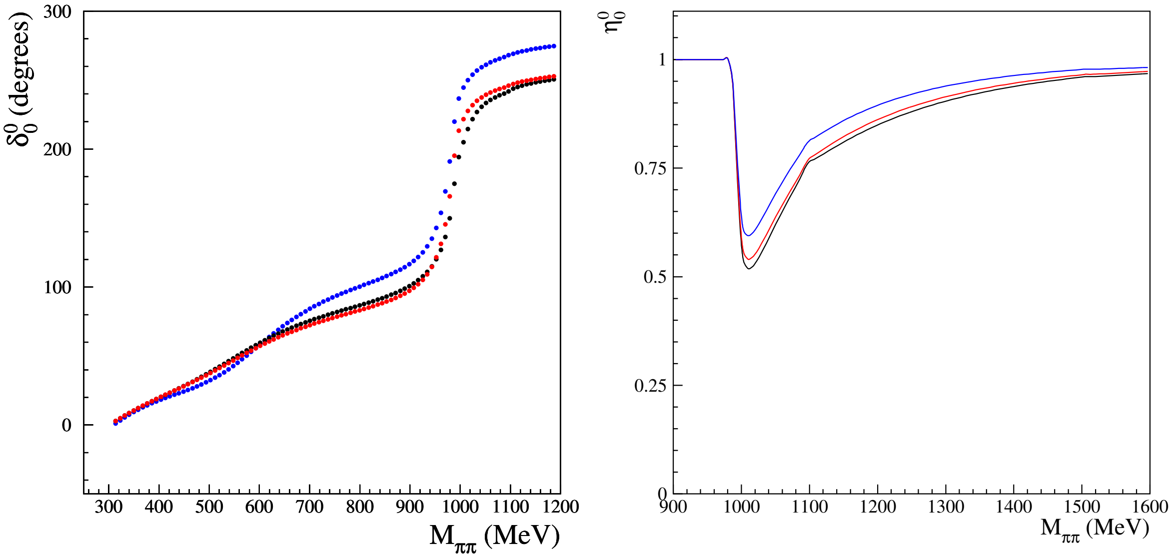

Figure 10: $\pi\pi$ scattering phase (left) and inelasticity η_0^0 (right). The curves from Ref. [14] are shown in black while red and blue lines represent the distributions obtained from fit K1 with M_σ fixed and free respectively.

is shifted by 50–100 MeV except for K5 and K6, where the χ^2 improves dramatically at the price of lowering the σ mass of $\sim$ 300 MeV. As shown in Fig. 10.left, the variation of M_σ produces a big deviation of δ_0^0, and the resulting curve is not able to describe $\pi\pi$ scattering data as in the case with fixed mass. For the inelasticity (Fig. 10.right) the differences between the two curves are smaller and, due to the large experimental errors, are both able to describe data.

The fit results for the VMD parametrization, reported in Tab. 2, are also pretty stable. The scale factor of the resonant contribution $\phi \to \rho\pi \to \pi^0\pi^0\gamma$, $\alpha_{\rho\pi}$, that we add as a free parameter of the fit reaches $\sim$60–70% of its expected value. Similarly, the coupling constants of the not resonant terms, $C_{\omega\pi}$ and $C_{\rho\pi}$, do not differ more than 20% from their expected values although $C_{\rho\pi}$ is determined with large errors. The maximum excursion is obtained for the phase of the ρ–ω mixing while we extract a precise measurement of the ω mass: $M_\omega = (782.5 \pm 0.3_{\,\rm fit} - 0.4_{\,\rm mod})$ MeV.

In Figs. 11, 12 we show the distributions of the data points for all slices of the Dalitz

M_σ fixed

Fit	$\alpha_{\rho\pi}$	$C_{\omega\pi}$ (GeV^{-2})	$\phi_{\omega\pi}$	$C_{\rho\pi}$ (GeV^{-2})	$\phi_{\rho\pi}$	δ_{b_ρ} ($^\circ$)	M_ω (MeV)
K1	0.58 ± 0.11	0.850 ± 0.010	0.46 ± 0.13	0.260 ± 0.185	3.11 ± 3.12	33.0 ± 9.7	782.52 ± 0.29
K2	0.68 ± 0.03	0.832 ± 0.003	0.30 ± 0.05	0.061 ± 0.211	3.14 ± 3.08	23.6 ± 4.1	782.20 ± 0.11
K3	0.66 ± 0.17	0.836 ± 0.004	0.33 ± 0.08	0.084 ± 0.056	3.14 ± 3.14	25.2 ± 6.2	782.26 ± 0.28
K4	0.72 ± 0.04	0.826 ± 0.003	0.21 ± 0.06	0.062 ± 0.003	3.14 ± 0.02	15.7 ± 3.4	782.12 ± 0.11
K5	0.71 ± 0.05	0.814 ± 0.003	0.22 ± 0.07	0.231 ± 0.054	0.00 ± 2.01	26.1 ± 3.7	781.91 ± 0.13
K6	0.81 ± 0.03	0.813 ± 0.003	0.21 ± 0.05	0.060 ± 0.006	3.12 ± 0.43	10.4 ± 1.8	781.91 ± 0.09
K7	0.74 ± 0.06	0.825 ± 0.002	0.53 ± 0.07	0.065 ± 0.006	3.14 ± 0.03	31.2 ± 2.1	782.10 ± 0.19
K8	0.64 ± 0.05	0.836 ± 0.002	0.38 ± 0.06	0.061 ± 0.005	3.14 ± 0.04	31.3 ± 2.4	782.28 ± 0.14
K9	0.62 ± 0.01	0.838 ± 0.006	0.27 ± 0.04	0.298 ± 0.126	3.13 ± 0.07	10.4 ± 6.5	782.41 ± 0.07
K10	0.58 ± 0.04	0.843 ± 0.004	0.30 ± 0.06	0.061 ± 0.003	3.14 ± 0.01	33.7 ± 4.8	782.48 ± 0.13

M_σ free

Fit	$\alpha_{\rho\pi}$	$C_{\omega\pi}$ (GeV^{-2})	$\phi_{\omega\pi}$	$C_{\rho\pi}$ (GeV^{-2})	$\phi_{\rho\pi}$	δ_{b_ρ} ($^\circ$)	M_ω (MeV)
K1	0.62 ± 0.05	0.852 ± 0.015	0.19 ± 0.15	0.065 ± 0.217	2.96 ± 0.61	32.8 ± 7.9	782.32 ± 0.21
K2	0.73 ± 0.22	0.831 ± 0.003	0.18 ± 0.06	0.272 ± 0.123	3.14 ± 1.69	4.1 ± 3.6	782.12 ± 0.13
K3	0.69 ± 0.14	0.834 ± 0.004	0.16 ± 0.06	0.069 ± 0.204	3.14 ± 2.55	15.8 ± 1.9	782.12 ± 0.24
K4	0.69 ± 0.07	0.828 ± 0.006	0.40 ± 0.10	0.060 ± 0.184	3.14 ± 3.10	27.0 ± 9.1	782.20 ± 0.30
K5	0.65 ± 0.05	0.829 ± 0.003	0.77 ± 0.05	0.299 ± 0.003	2.65 ± 0.24	36.1 ± 2.0	782.06 ± 0.12
K6	0.62 ± 0.05	0.830 ± 0.011	0.84 ± 0.18	0.131 ± 0.201	0.69 ± 0.19	62.0 ± 8.1	782.09 ± 0.24
K7	0.75 ± 0.09	0.823 ± 0.008	0.42 ± 0.20	0.060 ± 0.139	3.14 ± 2.07	23.6 ± 12.1	781.98 ± 0.25
K8	0.70 ± 0.10	0.836 ± 0.006	0.12 ± 0.08	0.089 ± 0.180	3.14 ± 1.64	14.6 ± 13.6	782.09 ± 0.18
K9	0.66 ± 0.12	0.837 ± 0.003	0.05 ± 0.09	0.235 ± 0.207	3.13 ± 2.27	2.6 ± 7.6	782.29 ± 0.09
K10	0.62 ± 0.14	0.842 ± 0.007	0.04 ± 0.16	0.060 ± 0.129	3.14 ± 2.45	17.6 ± 10.1	782.32 ± 0.12

Table 2: Fit results for the VMD parametrization in the kaon loop model. Different rows are for the different sets of parameters used for the $\sigma(600)$ and the elastic parameters of $\pi\pi$ and $K\overline{K}$ scattering. Top table is when constraining the mass of the $\sigma(600)$ to the indicated value, bottom table is when leaving also the mass of the $\sigma(600)$ free to vary.

plot with the fitting function overimposed for variant K1. The corresponding fit residuals are reported in Figs. 13 and 14. In Fig. 15.left the single bin contribution to the χ^2 of the fit is reported as a function of the position in the Dalitz plot. The distribution is reasonably flat, showing that the fitting function nicely reproduces the data over the entire area. To understand the relative importance of the different fitting terms, we plot in Fig. 15.right the composition for Fit K1 in the $M_{\pi\pi}$ variable. It is evident that, as expected, the VMD ($S\gamma$) term is dominating in the region below (above) 700 MeV. The interference term is concentrated around 600 MeV.

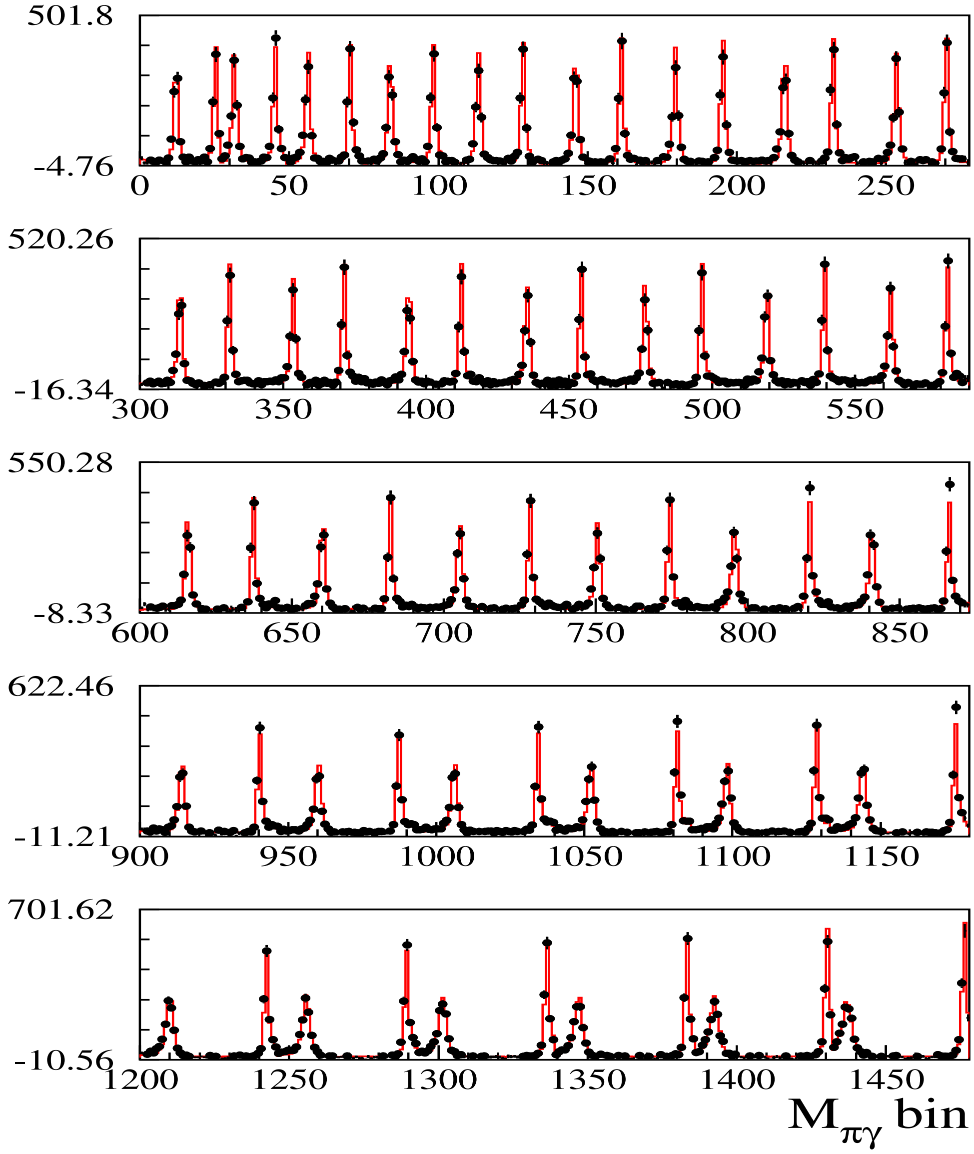

Figure 11: Fit Dalitz plot projections for kaon loop: the complete $M_{\pi\pi}$–$M_{\pi\gamma}$ plot is sliced in $M_{\pi\pi}$ and for each slice the $M_{\pi\gamma}$ projection is plotted, one after the other. Black dots are data while the red line represents the resulting shape from fit K1.

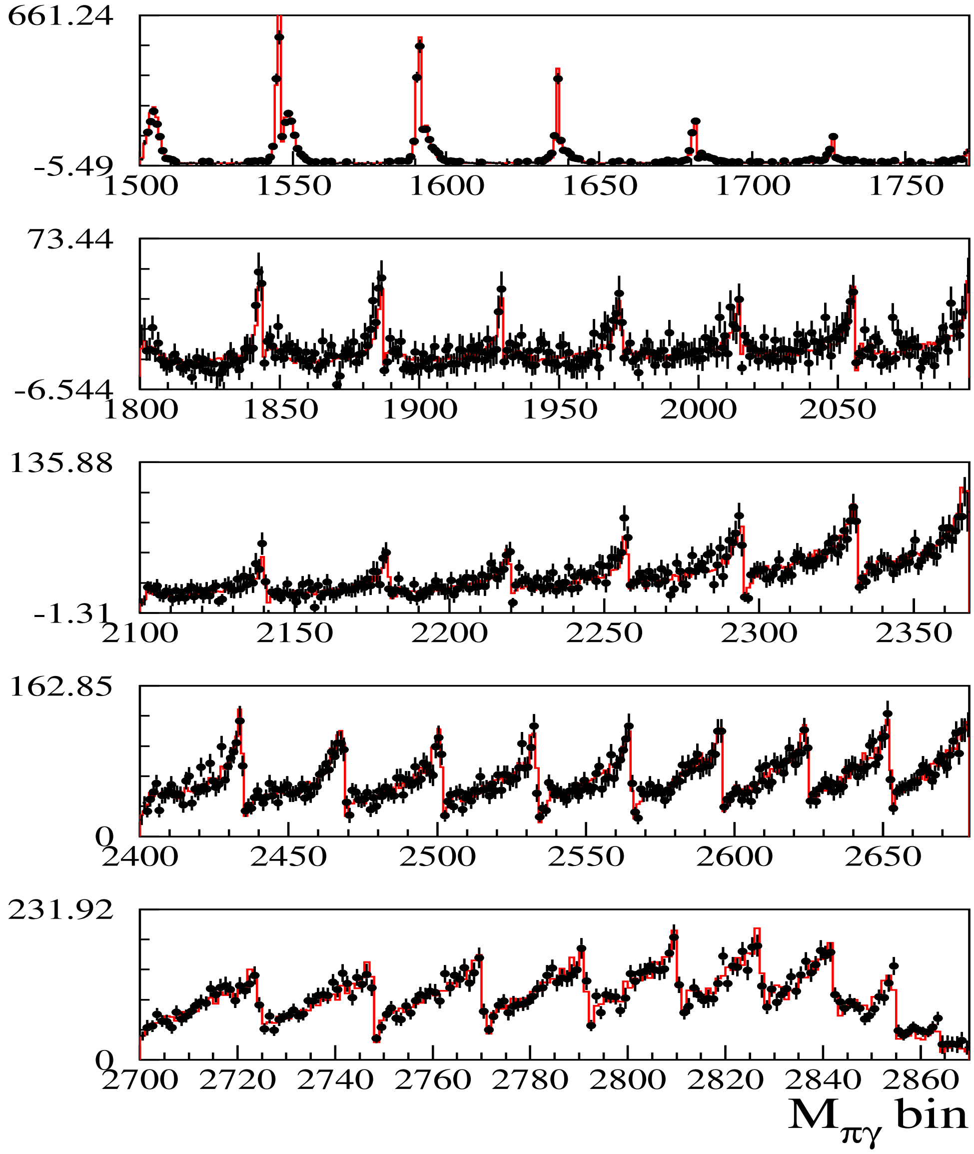

Figure 12: Fit Dalitz plot projections for kaon loop: the complete $M_{\pi\pi}$–$M_{\pi\gamma}$ plot is sliced in $M_{\pi\pi}$ and for each slice the $M_{\pi\gamma}$ projection is plotted, one after the other. Black dots are data while the red line represents the resulting shape from fit K1.

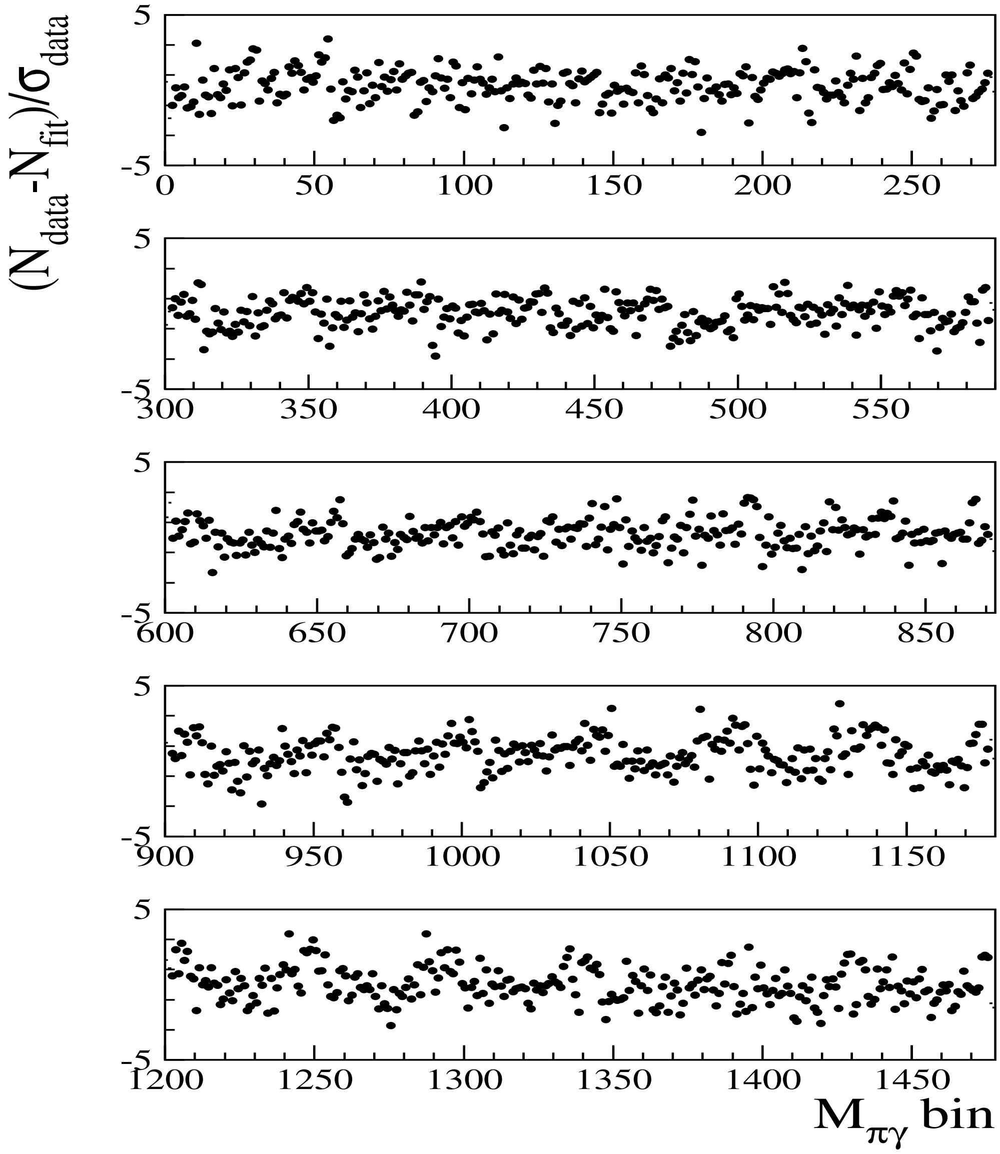

Figure 13: Fit residuals for K1 kaon loop model: the complete $M_{\pi\pi}$–$M_{\pi\gamma}$ plot is sliced in $M_{\pi\pi}$ and for each slice the $M_{\pi\gamma}$ projection is plotted, one after the other.

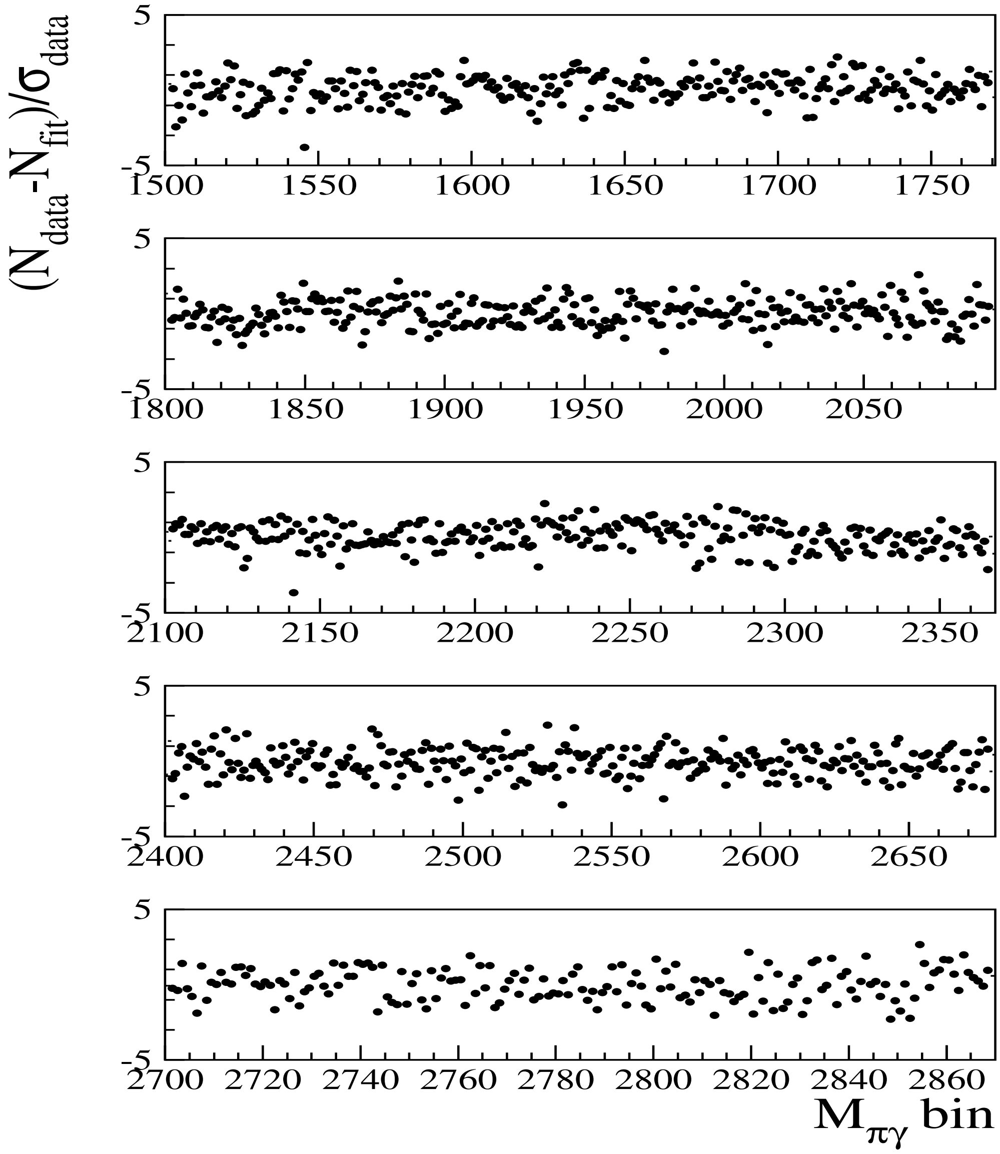

Figure 14: Fit residuals for K1 kaon loop model: the complete $M_{\pi\pi}$–$M_{\pi\gamma}$ plot is sliced in $M_{\pi\pi}$ and for each slice the $M_{\pi\gamma}$ projection is plotted, one after the other.

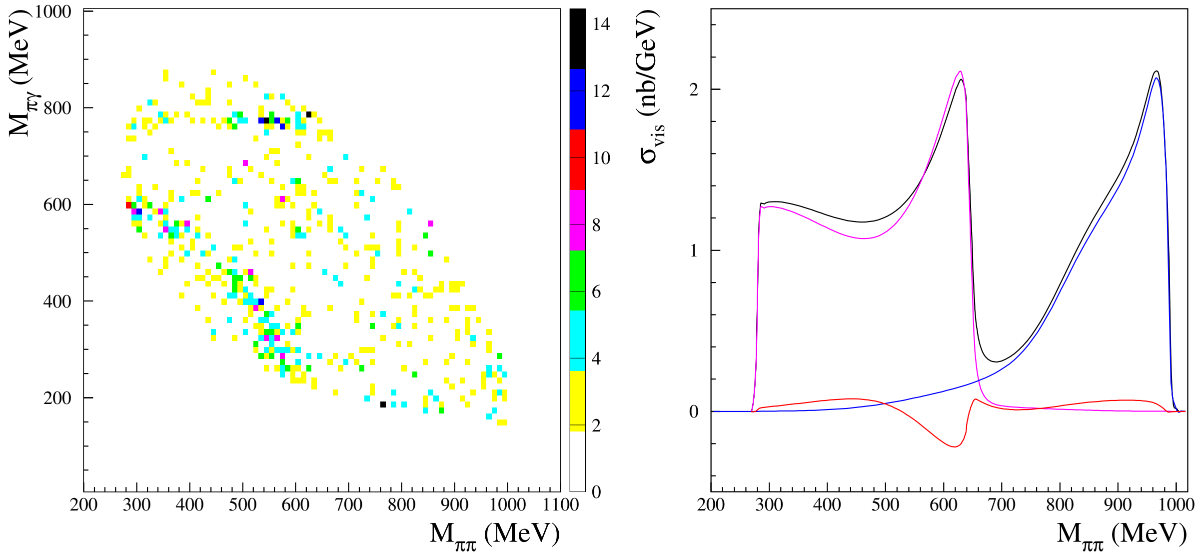

Figure 15: Kaon loop model, fit K1: χ^2 contributions in the Dalitz plot (left) and resulting $\pi^0\pi^0\gamma$ composition (right). The whole spectrum is shown in black, the $\omega\pi$ and $S\gamma$ contributions are reported in purple and blue respectively. The red line represents the interference term.

In Figs. 16.top the comparison of both VMD ans scalar contributions between the accepted fit results is shown. Stable resulting shapes are observed. By integrating the scalar term we get a born cross section for the process $\phi \to S\gamma \to \pi^0\pi^0\gamma$ of $(0.470\,^{+0.005}_{-0.013}\,{}_{\rm fit} - 0.027_{\rm mod})$ nb at peak ($M_\phi = 1019.46$ MeV). The first error is evaluated as the maximum excursion obtained when varying the fit errors on M_{f_0}, $g_{f_0\pi^+\pi^-}$ and $g_{f_0K^+K^-}$ by $\pm1\sigma$. By dividing for the ϕ production cross section at peak, $\sigma_0(\phi) = 12\pi\frac{\Gamma^\phi_{ee}}{\Gamma^\phi}\frac{1}{M^2_\phi}$ we derive the BR to be:

$$\mathrm{BR}(\phi \to S\gamma \to \pi^0\pi^0\gamma) = (1.07\,^{+0.01}_{-0.03}\,{}_{\rm fit} - 0.06_{\rm mod}) \times 10^{-4}, \tag{34}$$

in good agreement with our own direct measurement obtained with the same data set by excluding any interference with the VMD and subtracting the MC expected VMD contribution [4]. This result is also in agreement with the already published measurement performed with 2000 data [2].

Due to their interference, it is slightly more difficult to extract the single contribution

Fit	N1	N2
M_{f_0} (MeV)	984.7 ± 0.4	980.4 ± 0.6
$g_{f_0 K^+K^-}$(GeV)	0.40 ± 0.04	0.00 ± 0.06
$g_{f_0\pi^+\pi^-}$ (GeV)	1.31 ± 0.01	1.22 ± 0.01
$g_{\phi f_0 \gamma}$ (GeV^{-1})	2.61 ± 0.02	2.34 ± 0.03
a_0	4.19 ± 0.01	2.88 ± 0.05
a_1	1.31 ± 0.01	—
b_1 (rad)	-1.50 ± 0.02	—
$g_{\phi\sigma\gamma}$ (GeV^{-1})	—	-0.011 ± 0.001
$\chi^2/\mathrm{N_{dof}}$	2799/2672	2912/2673
$P(\chi^2)$	0.042	7×10^{-4}

Table 3: Fit results for the scalar term in the NS model. The two sets of parameters N1 and N2 are obtained with one and two scalar contribution respectively.

of $f_0(980)\gamma$ or $\sigma(600)\gamma$ terms. In Figs. 16.bottom we show their $M_{\pi\pi}$ distribution for the six accepted fits. The large variations of the single scalar meson contribution will reflect in a large model error in the extracted couplings.

To complete the overview of the fits performed on the kaon loop approach, we recall that we do not find acceptable χ^2 values when including only the $f_0(980)$ (see App. B).

5.2 Fit results for the NS model

In the case of the "no structure" model, we have tested the two possibilities described in Sec. 3.2 of using for the scalar term only a narrow meson pole, the $f_0(980)$, or adding also a broad meson, representing the $\sigma(600)$. We refer to the former (latter) case as N1 (N2). The fit results for the scalar term are reported in Tab. 3. An acceptable χ^2 probability is obtained for the N1 parametrization while the N2 description originates a too large χ^2 value and is therefore rejected. The coupling to $K\overline{K}$ pair is substantially reduced with respect to the KL model.

The fit results for the VMD parametrization, reported in Tab. 4, are stable but slightly different from the KL fit. In particular, the scalar factor for the $\phi \to \rho\pi \to \pi^0\pi^0\gamma$ contribution is 40% higher of its expected value, the $C_{\omega\pi}$ is real with a larger absolute

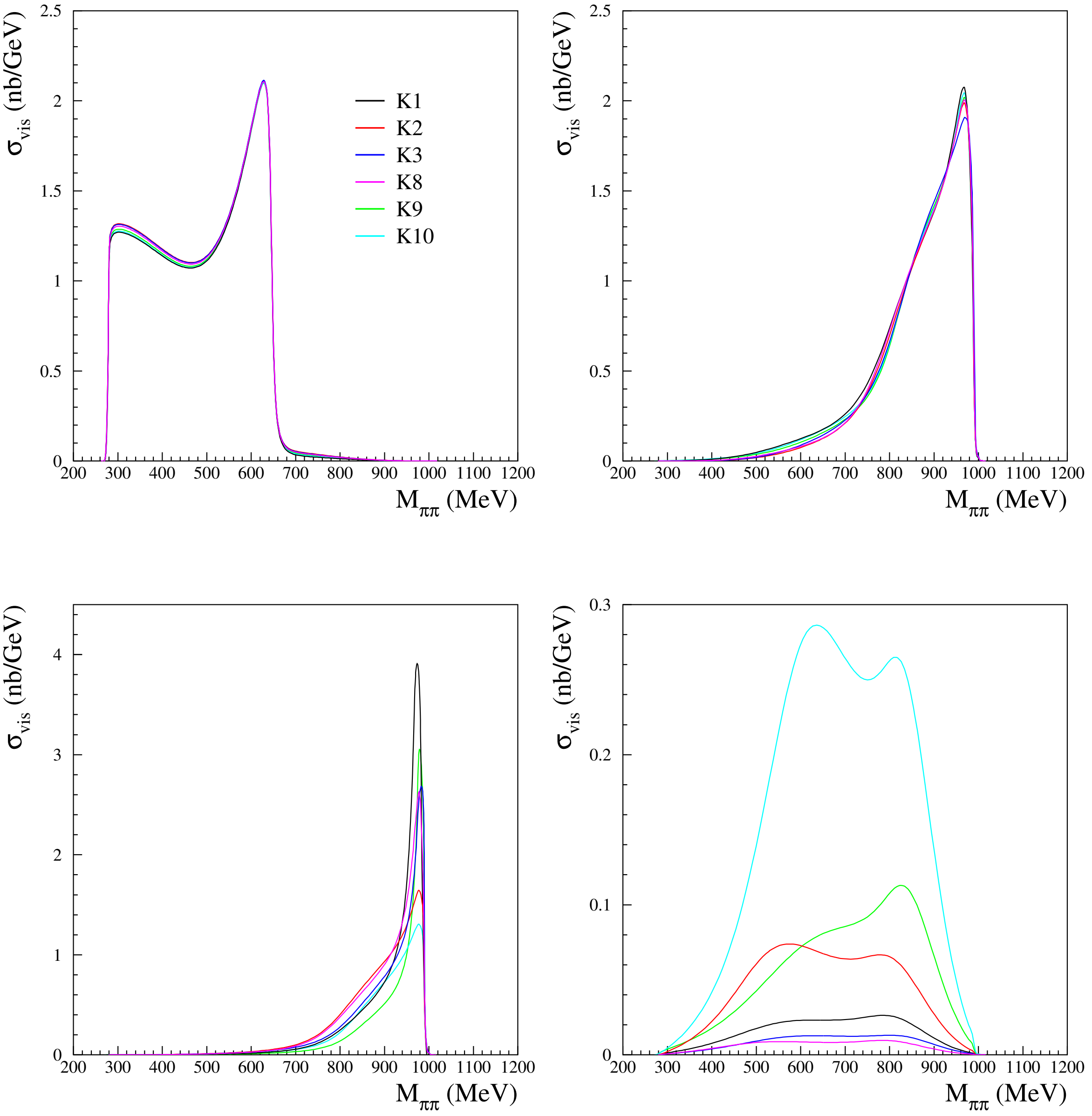

Figure 16: Comparison of fit results between the six accepted variants of the KL model: VMD (top-left), complete scalar contribution (top-right), $\phi \to f_0(980)\gamma$ (bottom-left) and $\phi \to \sigma(600)\gamma$ (bottom-right).

Fit	$\alpha_{\rho\pi}$	$C_{\omega\pi}$ (GeV^{-2})	$\phi_{\omega\pi}$	$C_{\rho\pi}$ (GeV^{-2})	$\phi_{\rho\pi}$	δ_{b_ρ} (°)	M_ω (MeV)
N1	1.43 ± 0.04	0.953 ± 0.003	0.00 ± 0.01	0.270 ± 0.039	3.11 ± 0.14	73.1 ± 1.6	781.80 ± 0.11
N2	1.11 ± 0.05	0.948 ± 0.003	0.00 ± 0.01	0.300 ± 0.003	2.85 ± 0.16	67.9 ± 1.0	782.03 ± 0.13

Table 4: Fit results for the VMD parametrization in the NS model. The two sets of parameters N1, N2 are obtained with one scalar, two scalars contribution respectively.

value and the phase δ_{b_ρ} is also increased to 70 degrees. The ω mass is determined with good precision but shifted of 0.7 MeV from the KL fit value. However, the distribution of the differential cross section for the VMD term shows a reasonable agreement with the kaon loop resulting shape (Fig. 23.left).

In Figs. 17, 18 the data distributions for all slices of the Dalitz plot are shown as black points while the red curve overimposed is the fitting function of variant N1. The corresponding fit residuals are reported in Figs. 19 and 20. The single bin contribution to the χ^2 of the fit is reported in Fig. 21.left, showing a reasonably flat distribution. The different components of the fit are reported in Fig. 21.right. Again, for $M_{\pi\pi} > 700$ MeV the scalar term is clearly dominant. However, differently from the KL case, the interference term gets negative in this region, so that the scalar term is slightly increased. We have also checked the distribution of the phase described in Sec. 3.2 (Fig. 22). While the starting slope and the behaviour at $M_{\pi\pi} \sim 980$ MeV are reasonable, an unexpected shape is observed for the intermediate mass values.

In Fig. 23.right an absolute comparison of the scalar term visible differential cross section between the best fits for the KL and NS model is shown. The general behaviour is the same although differences at a level of few %, mainly due to the interference term, can be noticed. This reflects in a slightly higher evaluation of the born cross section for the process $\phi \to S\gamma \to \pi^0\pi^0\gamma$ that gets the value of $(0.492 \pm 0.033_{\rm fit})$ nb. The fit error has been evaluated by varying of $\pm 1\sigma$ the most important fit parameters: the maximum variation observed from the central value determines this error. By dividing this cross section for σ_ϕ, evaluated at M_ϕ, we extract the BR to be:

$$\mathrm{BR}(\phi \to S\gamma \to \pi^0\pi^0\gamma) = (1.12 \pm 0.08_{\,\rm fit}) \times 10^{-4}\,, \tag{35}$$

which is $\sim 5\%$ higher than the one obtained with the KL fit. The NS and KL scalar shapes are compared in Fig. 23.right with the distribution obtained from the 2000 data $\pi^0\pi^0\gamma$ analysis [2]. The new spectra are lower than the old ones in the 600–800 MeV mass

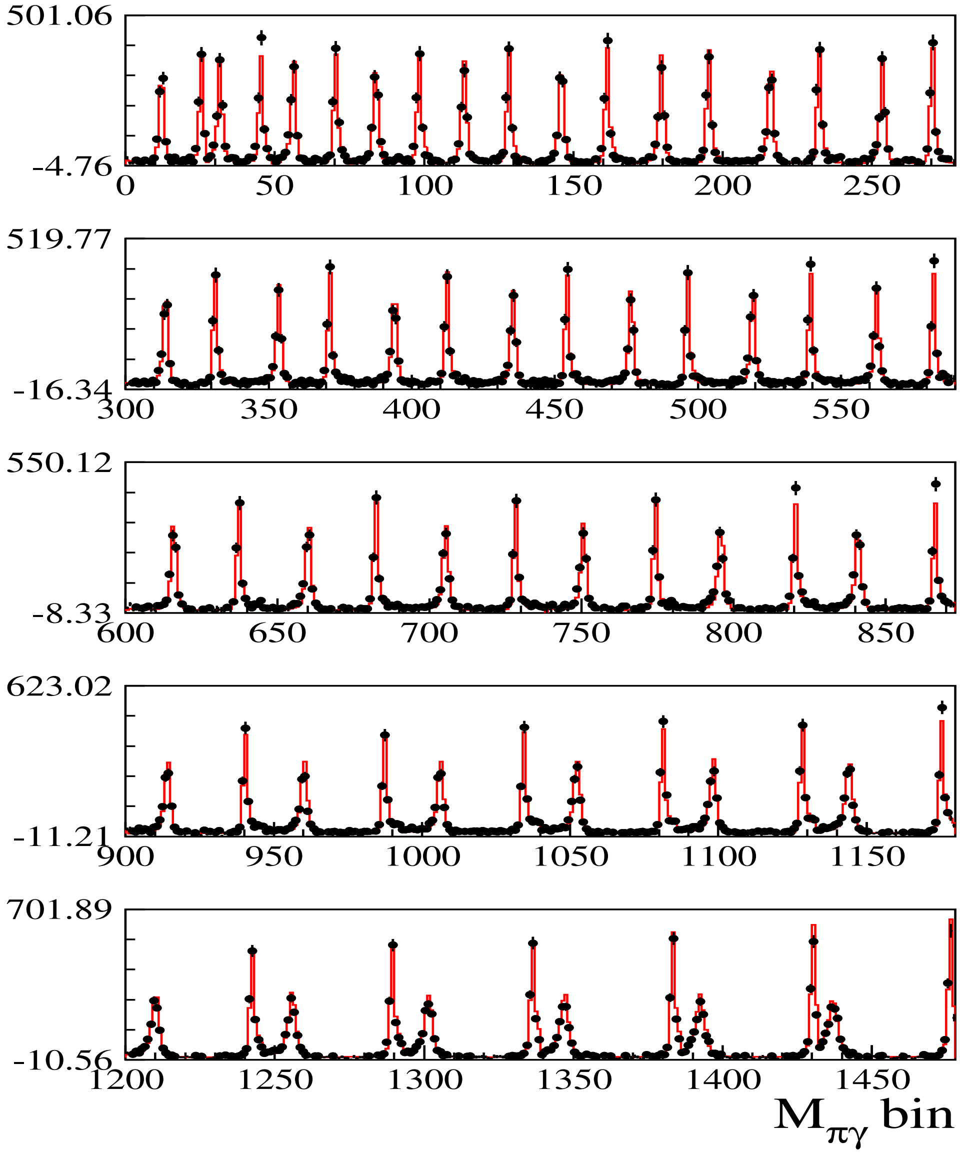

Figure 17: Fit Dalitz plot projections for NS model: the complete $M_{\pi\pi}$–$M_{\pi\gamma}$ plot is sliced in $M_{\pi\pi}$ and for each slice the $M_{\pi\gamma}$ projection is plotted, one after the other. Black dots are data while the red line represents the resulting shape from fit N1.

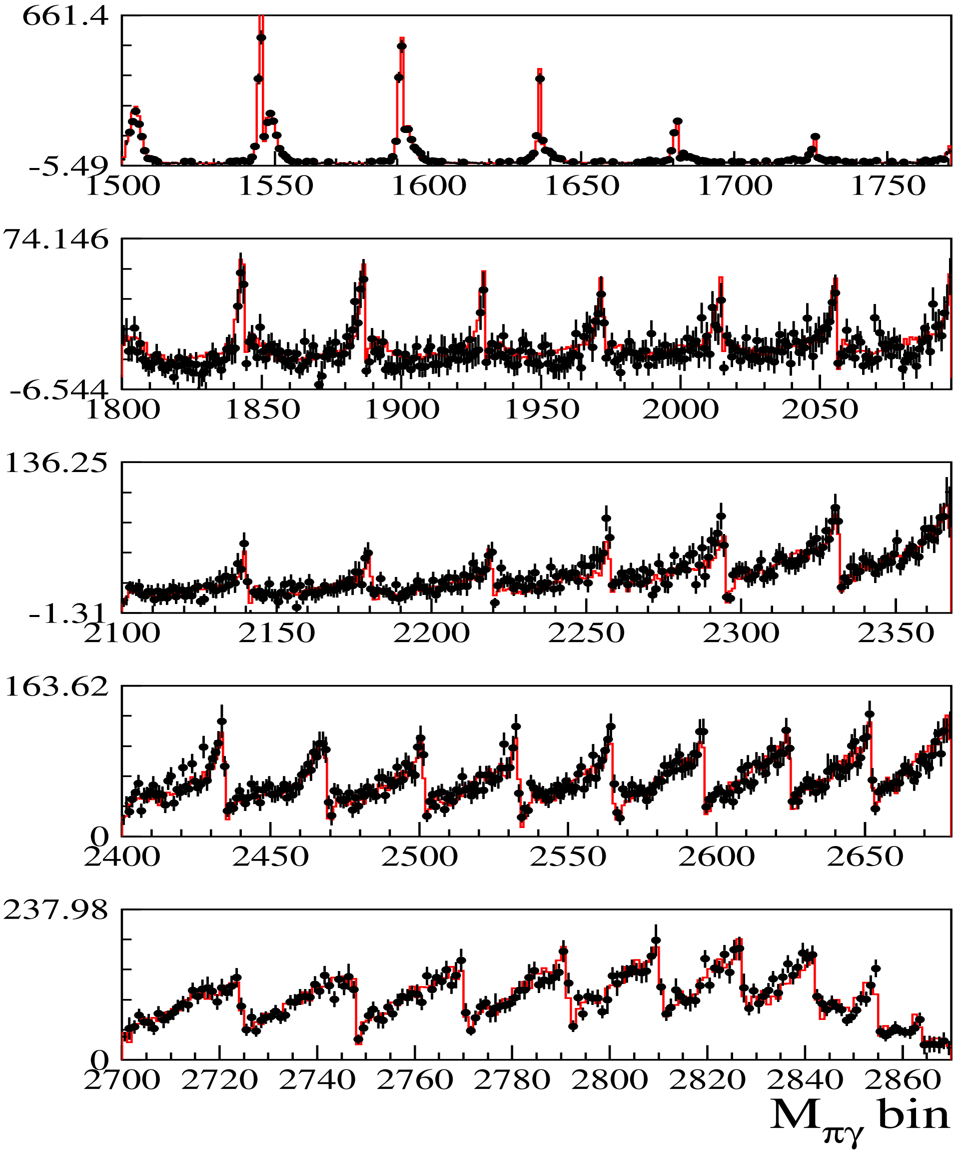

Figure 18: Fit Dalitz plot projections for NS model: the complete $M_{\pi\pi}$–$M_{\pi\gamma}$ plot is sliced in $M_{\pi\pi}$ and for each slice the $M_{\pi\gamma}$ projection is plotted, one after the other. Black dots are data while the red line represents the resulting shape from fit N1.

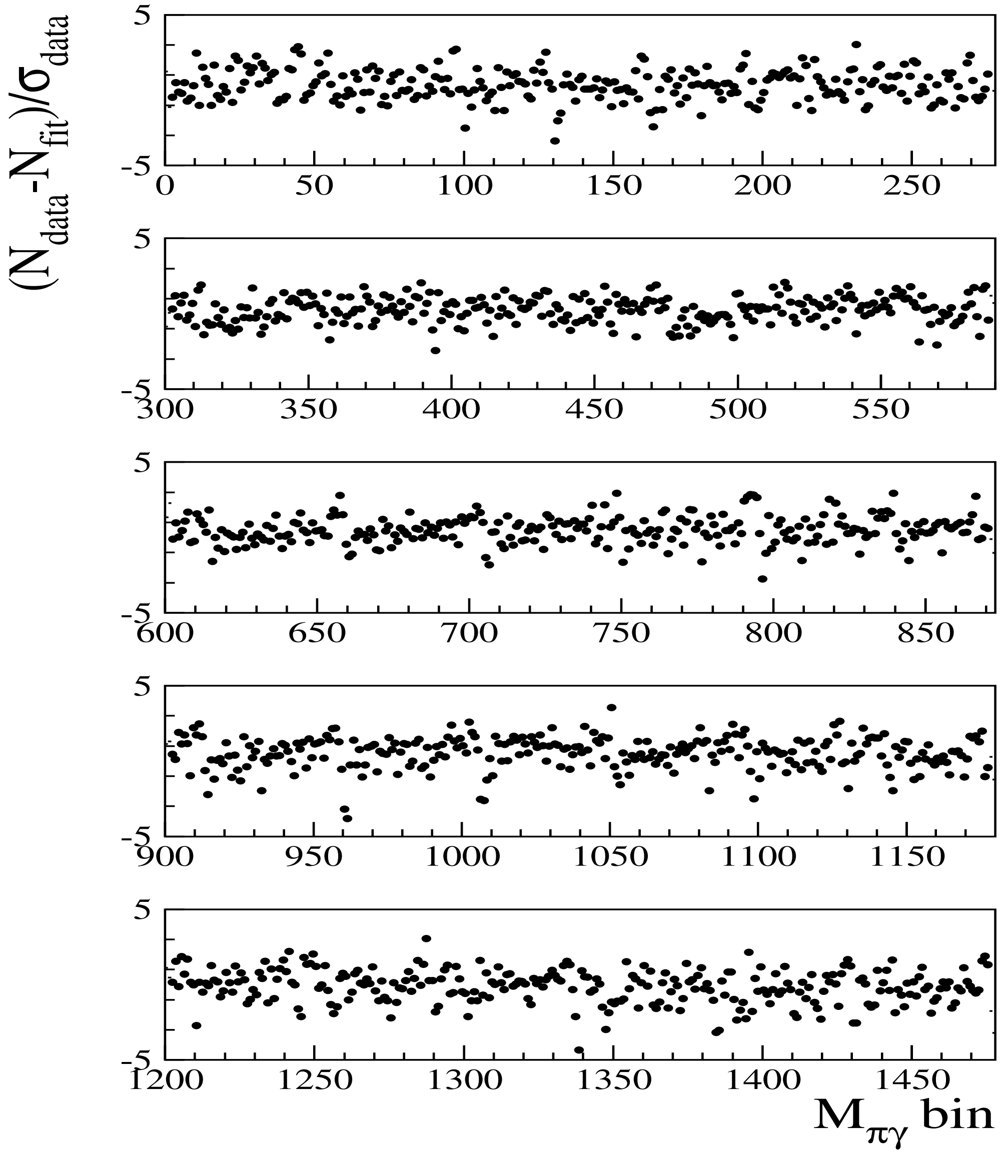

Figure 19: Fit residuals for N1 “no structure” model: the complete $M_{\pi\pi}$–$M_{\pi\gamma}$ plot is sliced in $M_{\pi\pi}$ and for each slice the $M_{\pi\gamma}$ projection is plotted, one after the other.

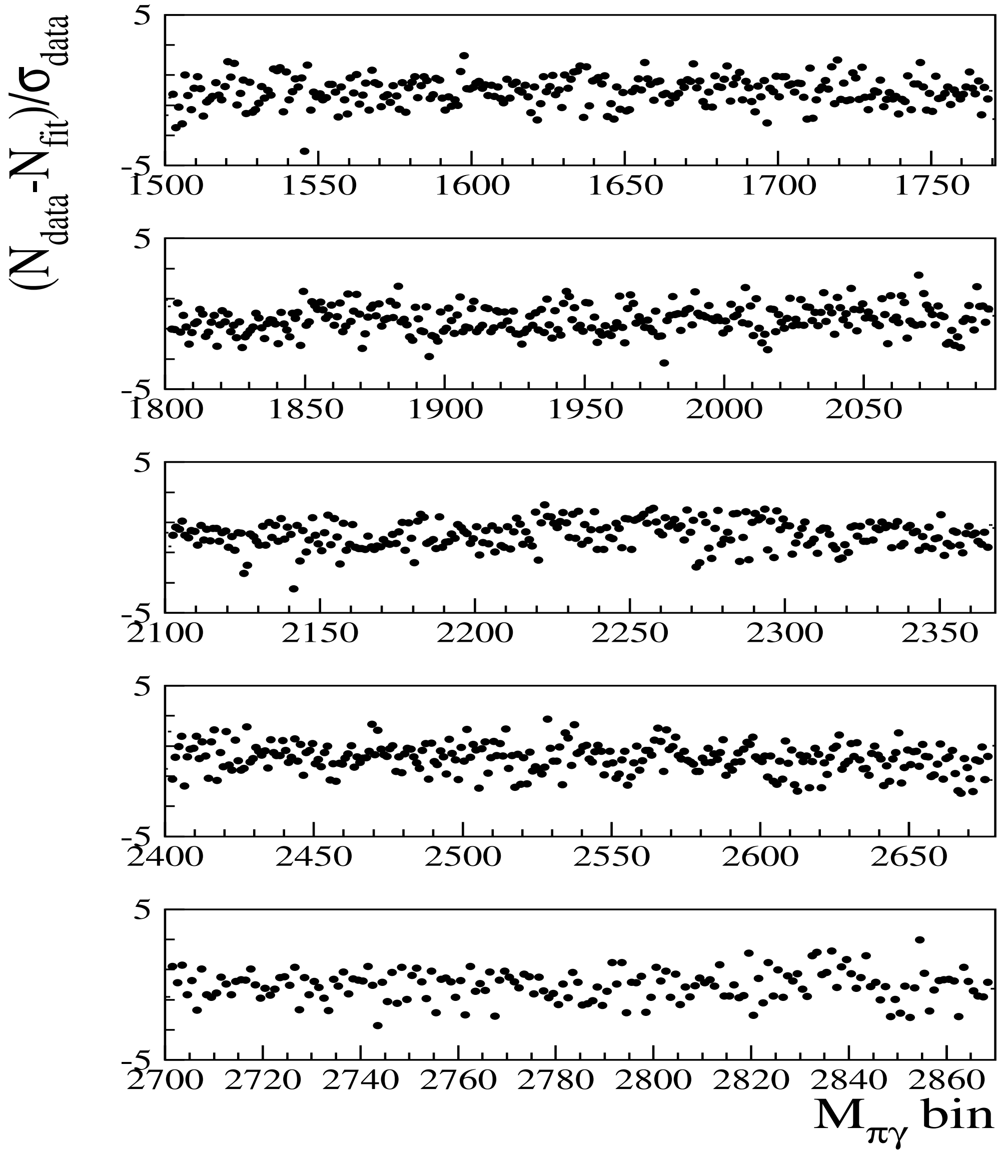

Figure 20: Fit residuals for N1 "no structure" model: the complete $M_{\pi\pi}$–$M_{\pi\gamma}$ plot is sliced in $M_{\pi\pi}$ and for each slice the $M_{\pi\gamma}$ projection is plotted, one after the other.

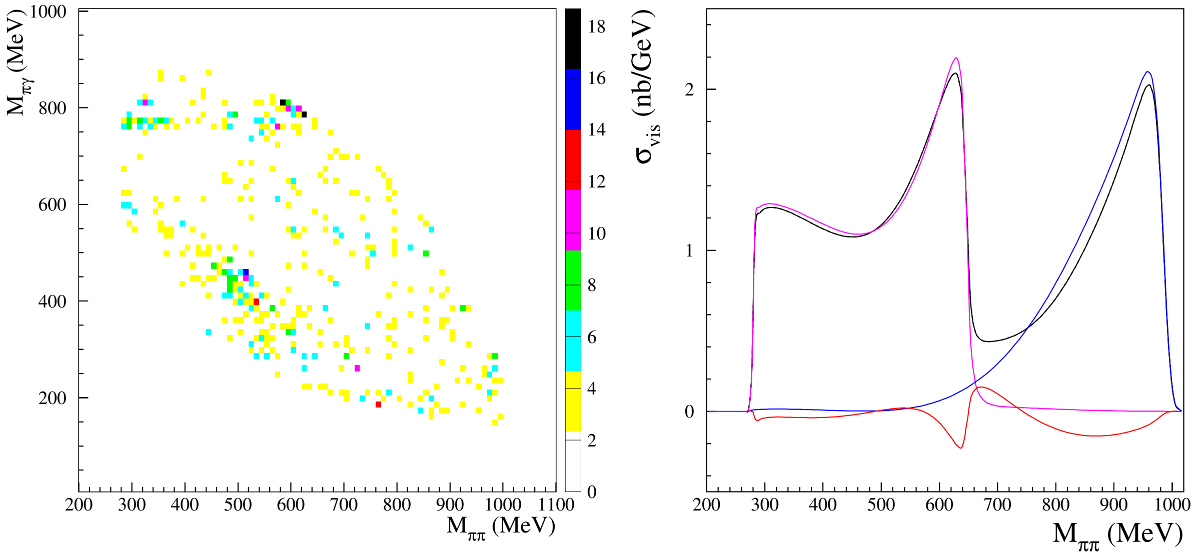

Figure 21: "No structure" model, fit N1: χ^2 contributions in the Dalitz plot (left) and resulting $\pi^0\pi^0\gamma$ composition (right). The whole spectrum is shown in black, the $\omega\pi$ and $S\gamma$ contributions are reported in purple and blue respectively. The red line represents the interference term.

region and the bump at small $M_{\pi\pi}$ values, resulting from the old $\sigma(600)$ parametrization, is not present anymore.

5.3 Fit systematics

A detailed study of the sources of systematics related to this analysis is reported in Ref. [4]. Most of these sources can give origin to variations of the fit results. For this reason, we have repeated the fit after changing in a proper way the relevant quantity. All the effects taken into account are listed below:

1. *Absolute normalization scale*
   The estimate of the event counting is directly related to two normalization constants: the integrated luminosity, $L_{\rm int}$, and the value of the ϕ leptonic width, Γ_{ee}. The fit has been repeated by changing the value of both quantities of $\pm 1\sigma$ ($\delta L_{\rm int}/L_{\rm int} = 0.6\%$, $\delta\Gamma_{ee}/\Gamma_{ee} = 1.7\%$).

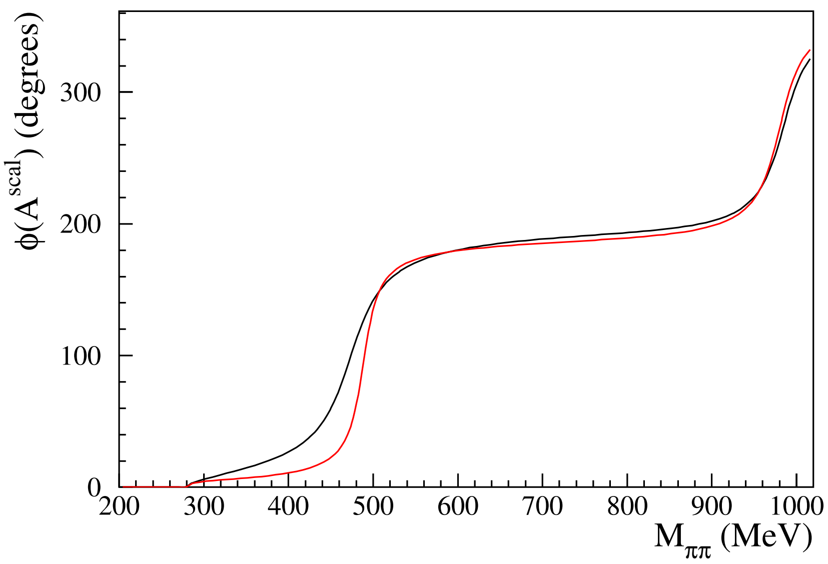

Figure 22: Phase of the scalar amplitude for the “no structure” model: the black curve is obtained when using N1 fit results, the red one using N2.

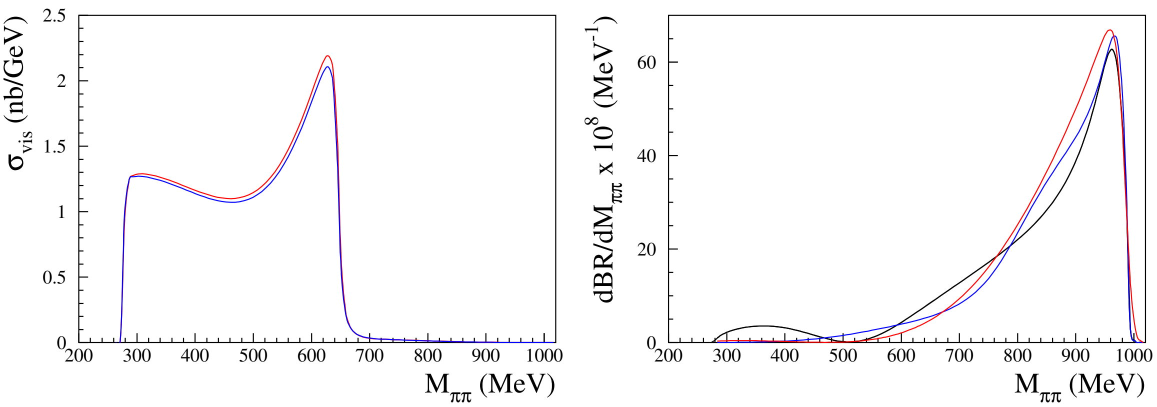

Figure 23: Comparison of the VMD (left) and scalar (right) contributions between the best fit for KL (blue) and NS (red) models. In the right panel, the scalar shape resulting from the published $\pi^0\pi^0\gamma$ analysis is shown in black.

2. *Beam energy scale*

   As explained before, the total energy scale has been shifted of +150 keV following the calibration performed with $\phi \to \eta\gamma$ events. To understand its effect on the fit, we have moved back the $\sqrt{s}$ value of the same amount.

3. *Cluster efficiency curve*

   The new parametrization curves of the cluster efficiency in the Montecarlo [27] have been used to evaluate anew the smearing matrix, the analysis efficiency and the background contribution. The fit has been repeated in these conditions.

4. *Kinematic fit: χ^2 cut*

   The analysis has been repeated after moving down the $\chi^2/\mathrm{N}_{\mathrm{dof}}$ cut from 5 to 3. In this way the analysis efficiency for $\omega\pi$ events is more dependent on the ISR tails, but the background quantity is largely reduced.

5. *Smearing matrix*

   According to the measured quantity of wrong photon pairing, the fraction of off-diagonal events in the smearing matrix has been increased by 8%.

6. *Folding of the interference term*

   In the standard fit we have used for the interference term the radiative corrections, the analysis efficiency and the smearing matrix obtained from $\omega\pi$ MC events. The fit is repeated by using the corresponding quantities estimated with $S\gamma$ events.

7. *Background subtraction*

   The scale factors obtained fitting the background-enriched distributions are applied to the residual background contamination.

The values of the fit parameters obtained in these new running conditions are reported in Tabs. 5, 6 for KL and NS fits respectively. The maximum variation of the central value is used to evaluate the corresponding systematic error.

5.4 Summary of fit results

We summarize in the following what found by this analysis. The most stable result is the contribution of the scalar term in the $\pi^0\pi^0\gamma$ final state. We measure a born cross section

Systematics source	M_{f_0} (MeV)	$g_{f_0 K^+K^-}$ (GeV)	$g_{f_0\pi^+\pi^-}$ (GeV)
K1 fit results	976.8 ± 0.3	3.76 ± 0.04	-1.43 ± 0.01
$\mathrm{L_{int}}$: $+1\sigma$	976.8 ± 0.3	3.74 ± 0.03	-1.42 ± 0.01
$\mathrm{L_{int}}$: -1σ	976.8 ± 0.4	3.78 ± 0.05	-1.43 ± 0.02
Γ_{ee}: $+1\sigma$	976.8 ± 0.6	3.70 ± 0.06	-1.42 ± 0.01
Γ_{ee}: -1σ	976.8 ± 0.4	3.82 ± 0.04	-1.44 ± 0.02
$\sqrt{s}$: 150 keV shift	976.9 ± 0.7	3.85 ± 0.07	-1.45 ± 0.02
Cluster efficiency curve	976.5 ± 0.3	3.68 ± 0.03	-1.41 ± 0.01
$\chi^2_{\mathrm{Fit2}}/\mathrm{N_{dof}} < 3$	976.5 ± 0.4	3.73 ± 0.04	-1.43 ± 0.01
Smearing matrix	976.2 ± 0.7	3.76 ± 0.07	-1.41 ± 0.02
Interf. with $S\gamma$ analysis	976.5 ± 0.7	3.72 ± 0.07	-1.42 ± 0.02
Background	977.7 ± 0.7	3.91 ± 0.07	-1.48 ± 0.01
Max. variation	$-0.6/+0.9$	$-0.08/+0.15$	$-0.02/+0.05$

Table 5: Fit results for the scalar term in the kaon loop model obtained when applying a systematic effect. In the first row the K1 fit results are reported for comparison.

Syst.	M_{f_0} (MeV)	$g_{f_0 K^+K^-}$ (GeV)	$g_{f_0\pi^+\pi^-}$ (GeV)	$g_{\phi f\gamma}$ (GeV^{-1})	a_0	a_1	b_1 (rad)
N1 fit	984.7 ± 0.4	0.40 ± 0.04	1.31 ± 0.01	2.61 ± 0.02	4.19 ± 0.01	1.31 ± 0.01	-1.50 ± 0.02
$\mathrm{L_{int}}$: $+1\sigma$	985.6 ± 0.3	1.02 ± 0.04	1.40 ± 0.01	2.92 ± 0.03	5.63 ± 0.06	2.91 ± 0.04	-0.64 ± 0.01
$\mathrm{L_{int}}$: -1σ	983.3 ± 0.3	0.62 ± 0.07	1.32 ± 0.01	2.62 ± 0.02	4.33 ± 0.01	1.56 ± 0.01	-1.21 ± 0.01
Γ_{ee}: $+1\sigma$	985.0 ± 1.0	0.76 ± 0.15	1.35 ± 0.02	2.78 ± 0.06	4.85 ± 0.22	1.98 ± 0.22	-0.90 ± 0.16
Γ_{ee}: -1σ	983.9 ± 0.4	0.20 ± 0.07	1.29 ± 0.01	2.56 ± 0.02	3.96 ± 0.01	1.10 ± 0.03	-1.75 ± 0.01
$\sqrt{s}$ shift	983.0 ± 0.2	0.73 ± 0.03	1.32 ± 0.01	2.66 ± 0.01	4.19 ± 0.01	1.31 ± 0.01	-1.55 ± 0.01
$\varepsilon_{\mathrm{cluster}}$	987.1 ± 0.3	0.11 ± 0.02	1.35 ± 0.01	2.70 ± 0.01	4.94 ± 0.01	1.96 ± 0.01	-1.06 ± 0.01
χ^2_{Fit2}	982.3 ± 1.0	0.63 ± 0.12	1.34 ± 0.01	2.55 ± 0.02	4.26 ± 0.11	1.54 ± 0.09	-1.20 ± 0.13
Smearing	982.3 ± 0.8	0.37 ± 0.13	1.28 ± 0.01	2.53 ± 0.02	3.77 ± 0.02	0.97 ± 0.04	-1.92 ± 0.12
Interf.	985.1 ± 1.3	0.73 ± 0.16	1.35 ± 0.01	2.75 ± 0.02	4.95 ± 0.06	2.22 ± 0.03	-0.81 ± 0.04
Bckg.	981.0 ± 0.7	0.77 ± 0.09	1.31 ± 0.01	2.55 ± 0.03	3.84 ± 0.02	1.20 ± 0.01	-1.44 ± 0.05
Max. var.	$-3.7/+2.4$	$-0.29/+0.62$	$-0.03/+0.09$	$-0.08/+0.31$	$-0.42/+1.44$	$-0.34/+1.60$	$-0.42/+0.86$

Table 6: Fit results for the scalar term in the "no structure" model obtained when applying a systematic effect. In the first row the N1 fit results are reported for comparison.

of:

$$\sigma_0(\phi \to S\gamma \to \pi^0\pi^0\gamma) = (0.470\,^{+0.005}_{-0.013\,\mathrm{fit}}\,^{+0.015}_{-0.008\,\mathrm{syst}}\,^{+0.022}_{-0.027\,\mathrm{mod}})\ \mathrm{nb} \qquad (36)$$

which corresponds to a branching ratio:

$$\mathrm{BR}(\phi \to S\gamma \to \pi^0\pi^0\gamma) = (1.07\,^{+0.01}_{-0.03\,\mathrm{fit}}\,^{+0.04}_{-0.02\,\mathrm{syst}}\,^{+0.05}_{-0.06\,\mathrm{mod}}) \times 10^{-4} \tag{37}$$

where the central values are given by the KL model with variant K1. The first error is statistical while the systematic errors take into account all changes reported in Sec. 5.3. The model error corresponds to the maximum variation from the central value observed when using the other six accepted fit results of the KL model and the N1 description.

For the extracted parameters we instead quote separately the results of the two theoretical description. For the KL model we extract:

$$M_{f_0} = (976.8 \pm 0.3_{\,\mathrm{fit}}\,^{+0.9}_{-0.6\,\mathrm{syst}} + 10.1_{\,\mathrm{mod}})\ \mathrm{MeV} \tag{38}$$

$$g_{f_0K^+K^-} = (3.76 \pm 0.04_{\,\mathrm{fit}}\,^{+0.15}_{-0.08\,\mathrm{syst}}\,^{+1.16}_{-0.48\,\mathrm{mod}})\ \mathrm{GeV} \tag{39}$$

$$g_{f_0\pi^+\pi^-} = (-1.43 \pm 0.01_{\,\mathrm{fit}}\,^{+0.01}_{-0.06\,\mathrm{syst}}\,^{+0.03}_{-0.60\,\mathrm{mod}})\ \mathrm{GeV} \tag{40}$$

$$R_{f_0} = \frac{g^2_{f_0K^+K^-}}{g^2_{f_0\pi^+\pi^-}} = 6.9 \pm 0.1_{\,\mathrm{fit}}\,^{+0.2}_{-0.1\,\mathrm{syst}}\,^{+0.3}_{-3.9\,\mathrm{mod}} \tag{41}$$

From these results we conclude that, in agreement with our own measurement in the $\pi^+\pi^-\gamma$ final state, we observe a strong coupling of the $f_0(980)$ to kaons which provides a good test of the 4-quark structure of this meson. The presence of a $\sigma(600)$ is needed to accurately describe the data. From the KL fit parameters the coupling of the ϕ to the $f_0\gamma$ can be extracted using the formula $\sqrt{\frac{3}{\alpha}\left(\frac{2M_\phi}{M^2_\phi - M^2_{f_0}}\right)^3 \Gamma_\phi\, 3\,\mathrm{BR}(\phi \to S\gamma \to \pi^0\pi^0\gamma)}$. The resulting value is:

$$g_{\phi f_0\gamma} = (2.78\,^{+0.02}_{-0.05\,\mathrm{fit}}\,^{+0.13}_{-0.05\,\mathrm{syst}} + 1.31_{\,\mathrm{mod}})\ \mathrm{GeV}^{-1} \tag{42}$$

For the NS description we instead find:

$$M_{f_0} = (984.7 \pm 0.4_{\,\mathrm{fit}}\,^{+2.4}_{-3.7\,\mathrm{syst}})\ \mathrm{MeV} \tag{43}$$

$$g_{f_0K^+K^-} = (0.40 \pm 0.04_{\,\mathrm{fit}}\,^{+0.62}_{-0.29\,\mathrm{syst}})\ \mathrm{GeV} \tag{44}$$

$$g_{f_0\pi^+\pi^-} = (1.31 \pm 0.01_{\,\mathrm{fit}}\,^{+0.09}_{-0.03\,\mathrm{syst}})\ \mathrm{GeV} \tag{45}$$

$$R_{f_0} = \frac{g^2_{f_0K^+K^-}}{g^2_{f_0\pi^+\pi^-}} = 0.09 \pm 0.02_{\,\mathrm{fit}}\,^{+0.44}_{-0.08\,\mathrm{syst}} \tag{46}$$

$$g_{\phi f_0\gamma} = (2.61 \pm 0.02_{\,\mathrm{fit}}\,^{+0.31}_{-0.08\,\mathrm{syst}})\ \mathrm{GeV}^{-1} \tag{47}$$

$$a_0 = \quad 4.19 \pm 0.01_{\,\mathrm{fit}}\,^{+1.44}_{-0.42\,\mathrm{syst}} \tag{48}$$

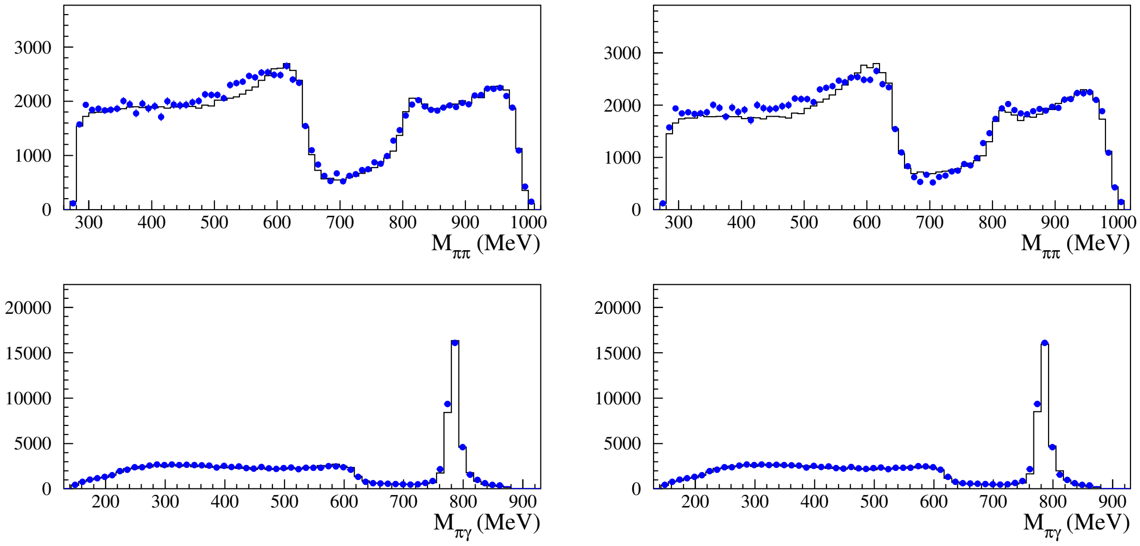

Figure 24: Dalitz plot projections for runs with $\sqrt{s} = 1019.75$ MeV: data are reported in blue dots while the solid line represents the fit result for KL (left) and NS (right) fits.

$$a_1 = \quad 1.31 \pm 0.01_{\,\mathrm{fit}}\,{}^{+1.60}_{-0.34}{}_{\,\mathrm{syst}} \tag{49}$$

$$b_1 = -1.50 \pm 0.02_{\,\mathrm{fit}}\,{}^{+0.86}_{-0.42}{}_{\,\mathrm{syst}} \tag{50}$$

As previously stated, the $f_0(980)$ mass value and the coupling to pions reasonably agree with the results of the KL approach. On the contrary, the coupling to kaons are significantly lowered. Also the coupling $g_{\phi f_0 \gamma}$ is smaller of a factor ≈ 2.5.

5.5 Extrapolation to other $\sqrt{s}$ values

As a last check, we extrapolate both KL and NS fit results to the four closest $\sqrt{s}$ points: 1019.55 MeV (42 pb^{-1}), 1019.65 MeV (77 pb^{-1}), 1019.85 MeV (100 pb^{-1}) and 1019.95 MeV (15 pb^{-1}), scaling for the integrated luminosity. The two Dalitz plot projections are then compared with the results obtained for $\sqrt{s} = 1019.75$ MeV (Fig. 24). As shown in Figs. 25 and 26, a good agreement is obtained in all distributions.

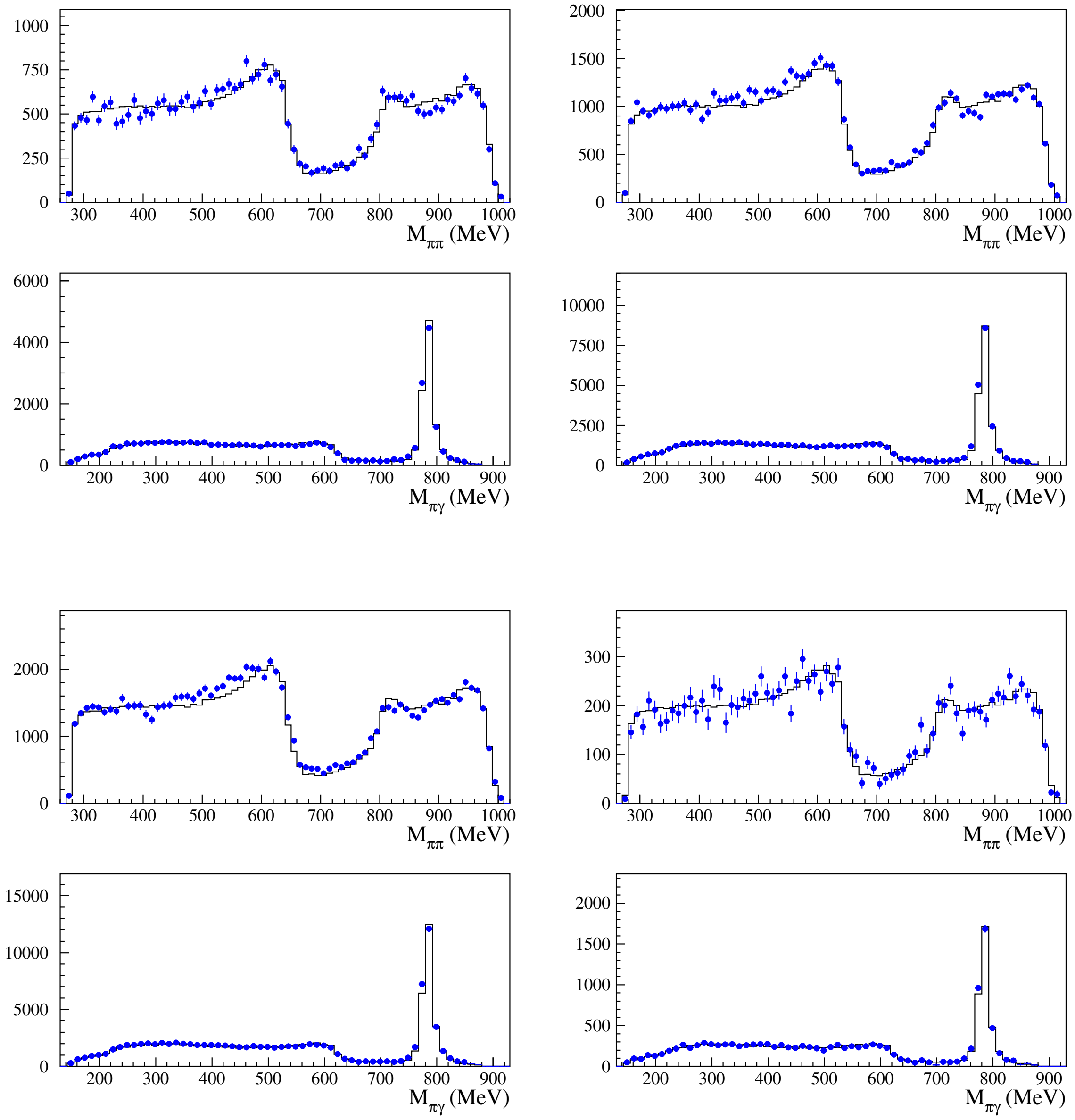

Figure 25: Dalitz plot projections for runs with different $\sqrt{s}$: 1019.55 MeV (top-left), 1019.65 MeV (top-right), 1019.85 MeV (bottom-left) and 1019.95 MeV (bottom-right). Data are reported in blue dots while the solid line represents the expected shape extrapolated from fit K1 of the kaon loop model.

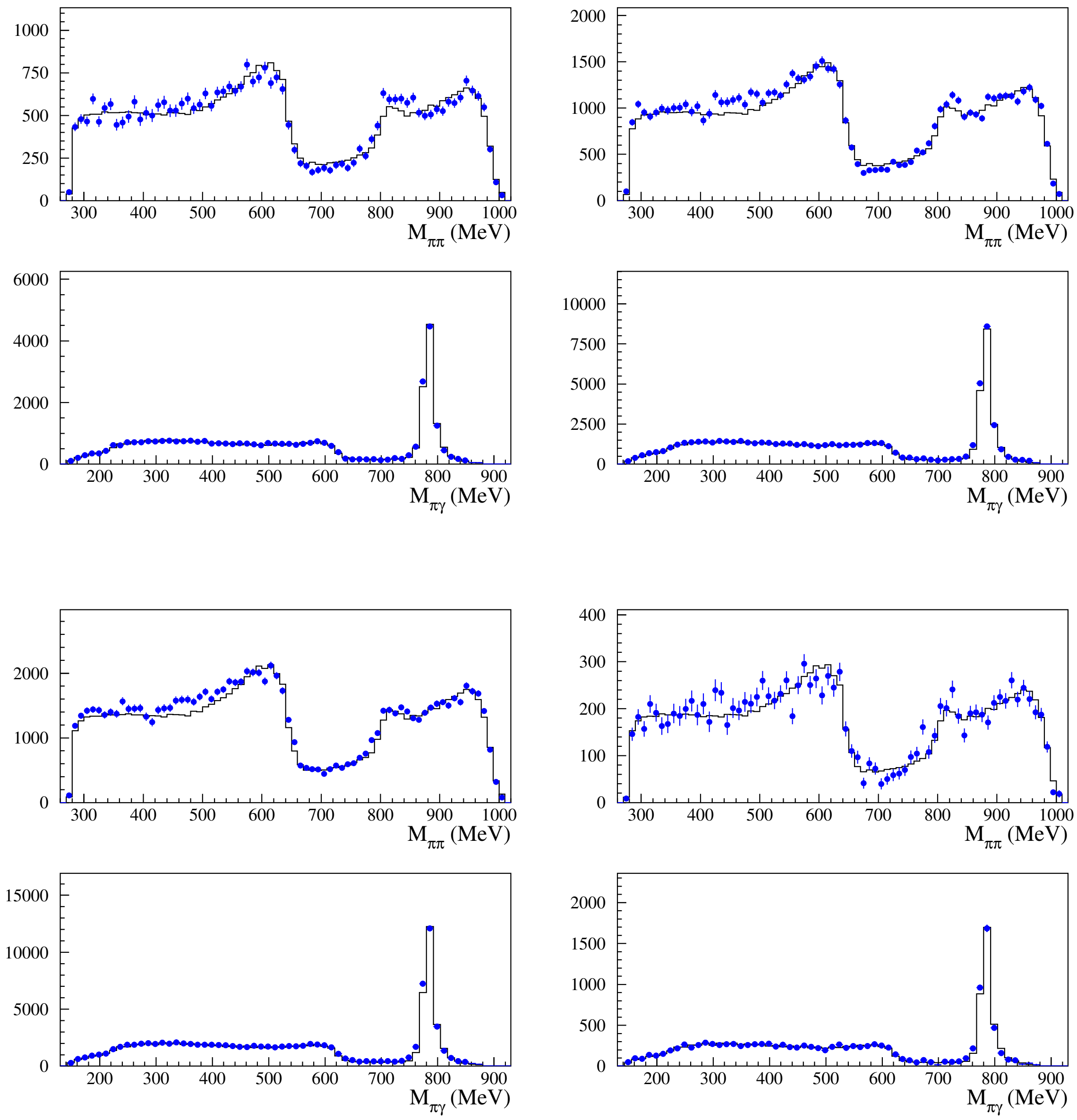

Figure 26: Dalitz plot projections for runs with different $\sqrt{s}$: 1019.55 MeV (top-left), 1019.65 MeV (top-right), 1019.85 MeV (bottom-left) and 1019.95 MeV (bottom-right). Data are reported in blue dots while the solid line represents the expected shape extrapolated from NS fit.

5.6 Comparison with $\pi^+\pi^-\gamma$ final state

The comparison between the results of this analysis and the ones of the $\pi^+\pi^-\gamma$ final state [1] is shown in this subsection. In particular, given the completely different composition of the irreducible backgrounds and of their interference with the scalar term, we concentrate only on the extracted couplings and cross section for the $\phi \to S\gamma$ process. To take into account the different final state, we multiply by two the cross section obtained in the neutral case. Therefore, the first comparison we make is of the total integrated cross section $\phi \to S\gamma \to \pi^+\pi^-\gamma$ which, after normalization by σ_ϕ, grants the BR($\phi \to S\gamma \to \pi^+\pi^-\gamma$). We quote a BR of $(2.14 \pm 0.14) \times 10^{-4}$ which has to be compared with $(2.1 \pm 0.4) \times 10^{-4}$, $(2.4 \pm 0.5) \times 10^{-4}$ found in the $\pi^+\pi^-\gamma$ analysis for the KL and NS model respectively. The BR looks in good agreement although it clearly shows that the precision of the neutral case is higher than the one of the $\pi^+\pi^-\gamma$ sample. However, this result hides the $M_{\pi\pi}$ dependence which has a much more pronounced discrepancy. In Fig. 27 the differential cross section as a function of $M_{\pi\pi}$ is shown for the KL and NS models. Large differences between the two cases can be observed although the neutral channel provides a much similar comparison between the two theoretical models.

The graphical difference shown by the differential cross section translates also in a difficult comparison of the coupling constants, summarized in Tab. 7. For the KL model, a reasonable agreement for the f_0 mass and for the coupling constants is observed. The difference in the $M_{\pi\pi}$ shape is related to the presence of the $\sigma(600)$ meson and of the P_K term in the neutral case which was instead not applied in the $\pi^+\pi^-\gamma$ final state. For the NS model instead, only the f_0 mass comes out as a comparable measurement. The shape is really distorted by the presence of the continuum background which is described by the free parameters a_0, a_1 and b_1. Not further conclusions can be drawn by these comparisons. The possibility to make a combined fit to the two final states is appealing to constrain in a more conclusive ways the models under consideration.

6 Conclusions

We have carried out an analysis of the $\pi^0\pi^0\gamma$ final state which has the novelty of not separating on an event-by-event basis the two main production mechanisms, the VMD and $S\gamma$ processes. The high collected statistics (145 pb^{-1} at 1019.75 MeV) allowed us to

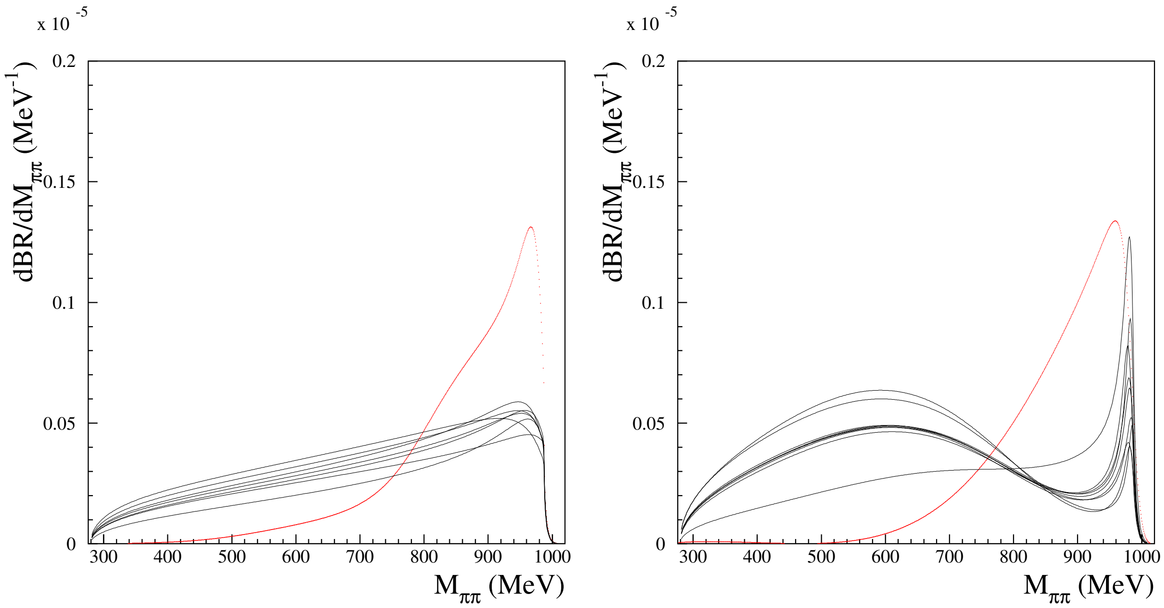

Figure 27: Comparison of the scalar shape obtained with the $\pi^+\pi^-\gamma$ (black) and $\pi^0\pi^0\gamma$ (red) final state for both KL (left) and NS (right) models. For the charged channel, the different curves are obtained by varying the fit parameters to their minimum and maximum values.

Model	Fit parameters	$\phi \to \pi^+\pi^-\gamma$	$\phi \to \pi^0\pi^0\gamma$
KL	M_{f_0}(MeV)	980–987	$976.8^{+10.1}_{-\ 0.6}$
	$g_{f_0 K^+K^-}$ (GeV)	5.0–6.3	$3.76^{+1.16}_{-0.49}$
	$g_{f_0\pi^+\pi^-}$ (GeV)	3.0–4.2	$-1.43^{+0.03}_{-0.60}$
	R_{f_0}	2.2–2.8	$6.9^{+0.4}_{-3.9}$
NS	M_{f_0}(MeV)	973–981	984.7 ± 2.4
	$g_{f_0 K^+K^-}$ (GeV)	1.6–2.3	$0.40^{+0.62}_{-0.29}$
	$g_{f_0\pi^+\pi^-}$ (GeV)	0.9–1.1	$1.31^{+0.09}_{-0.03}$
	R_{f_0}	2.6–4.4	$0.09^{+0.45}_{-0.08}$
	$g_{\phi f_0\gamma}$ GeV^{-1}	1.2–2.0	$2.61^{+0.31}_{-0.08}$

Table 7: Comparison of fit results for both KL and NS models using charged and neutral $\pi\pi\gamma$ final state.

fit with two different theory models the Dalitz plot distribution. In the kaon loop model, the two low mass scalars $f_0(980)$ and $\sigma(600)$ are required to adequately fit the data. Ten different configurations of the model are tested; six of them show a $P(\chi^2) > 1\%$ and are therefore accepted. In the case of the no structure model, we instead find an acceptable fit only in the case of a single $f_0(980)$ meson. However, in this description the low mass $M_{\pi\pi}$ behaviour is described by the three free parameters a_0, a_1 and b_1 representing the continuum background.

We obtain a stable branching ratio of the $\phi \to \pi^0\pi^0\gamma$ process:

$$\mathrm{BR}(\phi \to S\gamma \to \pi^0\pi^0\gamma) = (1.07\,^{+0.01}_{-0.03\,\mathrm{fit}}\,^{+0.04}_{-0.02\,\mathrm{syst}}\,^{+0.05}_{-0.06\,\mathrm{mod}}) \times 10^{-4}\,.$$

The last error reflects the maximum variation observed when changing the fit model. This result is in agreement with the exclusive analysis carried out in the same data set and with our old published measurement.

The extracted couplings show that the kaon loop model provides a stable description of the data with large couplings of the ϕ to the $f_0(980)$ and of the $f_0(980)$ to kaons, in agreement with what found in the $\pi^+\pi^-\gamma$ final state. Therefore, these results add evidences to a 4-quark structure of the $f_0(980)$ meson. On the other hand, in the fit with the no structure model, the same couplings gets substantially reduced and the $f_0(980)$ looks a much narrower object. However, the physical interpretation is somehow hidden by the presence of the continuum background which results different from the ones found in the $\pi^+\pi^-\gamma$ final state.

Acknowledgements

We want to thank many people which helped us in understanding these processes and in focusing our analysis towards a more solid conclusion. In particular, we are in debt with N. N. Achasov and A. V. Kiselev to have shown in a continuous way how to proper treat the theoretical problems hidden in various point. Moreover, we cannot forget G. Isidori, L. Maiani and S. Pacetti to have test most of the cross-section we use in the generators and be always friendly with us. We have also to thank P. Gauzzi for the joint-development of the $e^+e^- \to \omega\pi^0$ generator, M. Palutan and T. Spadaro for giving us the new photon efficiency curves, M. Dreucci and M. Antonelli for the ISR generator. Finally we acknowledge the help of C. Bini in the comparison of our results with the $\pi^+\pi^-\gamma$ analysis.

A Vector Meson Dominance coefficients

Here the expression of the coefficients used in Eq. 2 are explicitely reported. The variables m and $m_{\pi\gamma}$ represent the $\pi^0\pi^0$ and the $\pi^0\gamma$ invariant mass respectively, while s is the square of the total energy of the $\pi^0\pi^0\gamma$ system.

$$\begin{aligned} F_1(m^2, m_{\pi\gamma}^2) \; = \; & m_{\pi_0}^8 + 2\,m^2 m_{\pi_0}^4 m_{\pi\gamma}^2 - 4\,m_{\pi_0}^6 m_{\pi\gamma}^2 + 2\,m^4 m_{\pi\gamma}^4 - 4\,m^2 m_{\pi_0}^2 m_{\pi\gamma}^4 \\ & +6\,m_{\pi_0}^4 m_{\pi\gamma}^4 + 2\,m^2 m_{\pi\gamma}^6 - 4\,m_{\pi_0}^2 m_{\pi\gamma}^6 + m_{\pi\gamma}^8 - 2\,m_{\pi_0}^6 s \\ & -2\,m^2 m_{\pi_0}^2 m_{\pi\gamma}^2 s + 2\,m_{\pi_0}^4 m_{\pi\gamma}^2 s - 2\,m^2 m_{\pi\gamma}^4 s + 2\,m_{\pi_0}^2 m_{\pi\gamma}^4 s \\ & -2\,m_{\pi\gamma}^6 s + m_{\pi_0}^4 s^2 + m_{\pi\gamma}^4 s^2 \end{aligned} \tag{51}$$

$$\begin{aligned} F_2(m^2, m_{\pi\gamma}^2) \; = \; & m_{\pi_0}^8 - m^6 m_{\pi\gamma}^2 + 2\,m^4 m_{\pi_0}^2 m_{\pi\gamma}^2 + 2\,m^2 m_{\pi_0}^4 m_{\pi\gamma}^2 - 4\,m_{\pi_0}^6 m_{\pi\gamma}^2 \\ & -4\,m^2 m_{\pi_0}^2 m_{\pi\gamma}^4 + 6\,m_{\pi_0}^4 m_{\pi\gamma}^4 + 2\,m^2 m_{\pi\gamma}^6 - 4\,m_{\pi_0}^2 m_{\pi\gamma}^6 + m_{\pi\gamma}^8 \\ & +m^2 m_{\pi_0}^4 s - 2\,m_{\pi_0}^6 s + 2\,m^4 m_{\pi\gamma}^2 s - 4\,m^2 m_{\pi_0}^2 m_{\pi\gamma}^2 s \\ & +2\,m_{\pi_0}^4 m_{\pi\gamma}^2 s - m^2 m_{\pi\gamma}^4 s + 2\,m_{\pi_0}^2 m_{\pi\gamma}^4 s - 2\,m_{\pi\gamma}^6 s - m_{\pi_0}^4 s^2 \\ & -m^2 m_{\pi\gamma}^2 s^2 + 2\,m_{\pi_0}^2 m_{\pi\gamma}^2 s^2 + m_{\pi\gamma}^4 s^2 \end{aligned} \tag{52}$$

$$F_3(m^2, m_{\pi\gamma}^2) = \frac{(m_{\pi\gamma}^2 - m_{\pi_0}^2)^2 s - (s - m^2)^2 m_{\pi\gamma}^2}{s - m^2} \tag{53}$$

B Kaon loop fit results with a single scalar

To test the fit results of the kaon loop model with a single scalar we cannot use the new Achasov's parametrization, since the shape of the δ_0^0 strongly depends on the presence of the $\sigma(600)$ meson. We have therefore used the old KL parametrization [11], already used to fit 2000 data. Differently from the old analysis, we have fit the Dalitz plot instead of the simple $M_{\pi\pi}$ distribution. The results, compared with the old published ones, are reported in Tab. 8. The two sets of parameters are in excellent agreement; note that in case of a single scalar the sign of the coupling is irrelevant. In both cases the χ^2 of the fit is not acceptable, showing the need of introducing a $\sigma(600)$ contribution. This is also visible in Fig. 28, where the data-fit comparison is shown.

Data set	M_{f_0} (MeV)	$g_{f_0 K^+K^-}$ (GeV)	$g_{f_0\pi^+\pi^-}$ (GeV)	$\chi^2/\mathrm{N_{dof}}$
2000	962 ± 4	4.0 ± 0.2	2.2 ± 0.1	109.5/34
2001/2002	962.7 ± 0.2	4.24 ± 0.02	-2.14 ± 0.01	4285/2676

Table 8: Fit results for the KL fit with a single scalar for both 2000 and 2001/2002 data sets.

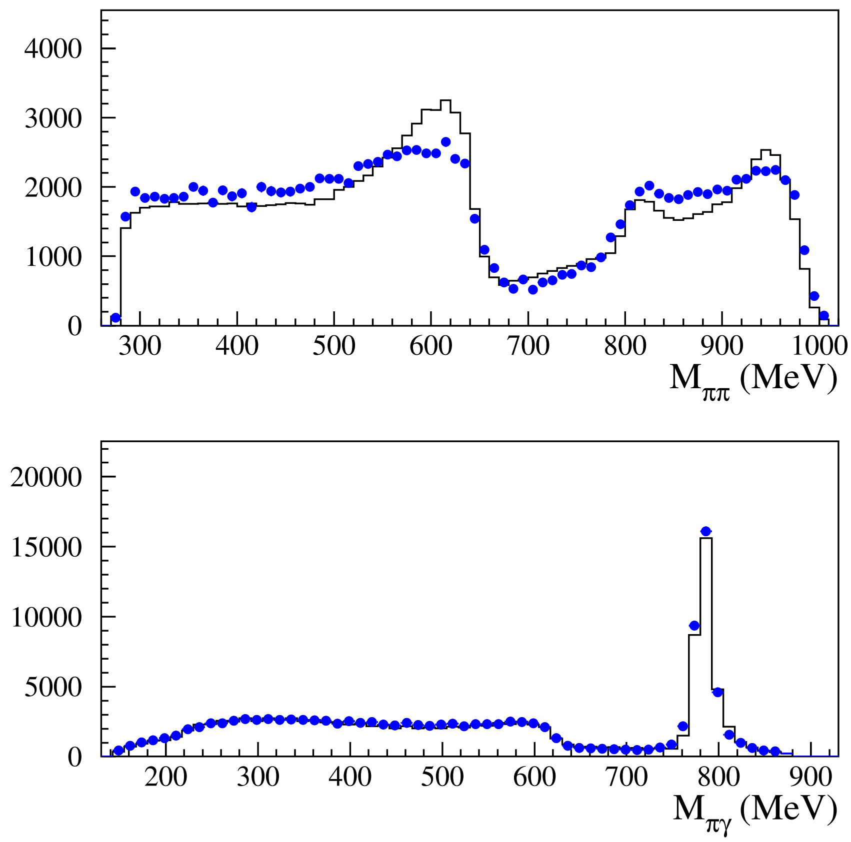

Figure 28: Dalitz plot projections for the KL fit with a single scalar. Data are reported in blue dots while the solid line represents the fit result.

References

[1] F. Ambrosino *et al.*, Phys. Lett. B 634 (2006) 148.

[2] A. Aloisio *et al.*, Phys. Lett. B 537 (2002) 21-27.

[3] A. Aloisio *et al.*, Phys. Lett. B 536 (2002) 209.

[4] S. Giovannella and S. Miscetti, KLOE Memo 319 (2005).

[5] V. M. Aulchenko *et al.*, Nucl. Phys. B 569 (2000) 158-182.

[6] V. M. Aulchenko *et al.*, J. Exp. Th. Phys. 90 (2000) 927-938.

[7] N. N. Achasov and V. V. Gubin, Phys. Rev. D63 (2001) 094007.

[8] N. N. Achasov and A. V. Kiselev, private communication following [9] and [7].

[9] M. N. Achasov *et al.*, Phys. Rev. D 68 (2003) 052006.

[10] N. N. Achasov and V. N. Ivanchenko, Nucl. Phys. B 315 (1989) 465-476.

[11] N. N. Achasov and V. V. Gubin, Phys. Rev. D 56 (1997) 4084.

[12] G. Isidori, L. Maiani, M. Nicolaci and S. Pacetti, J. High Energy Phys. 05 (2006) 049

[13] M. Boglione and M. R. Pennington, Eur. Phys. J. C 30 (2003) 503.

[14] N. N. Achasov and A. V. Kiselev, Phys. Rev. D 73 (2006) 054029.

[15] C. Bini, KLOE Note 207 (2005).

[16] N. N. Achasov and G. N. Shestakov, Phys. Rev. D 49 (1994) 5779.

[17] B. Hyams *et al.*, Nucl. Phys. B 64 (1973) 134.

[18] P. Estabrooks and A. D. Martin, Nucl. Phys. B 79 (1974) 301.

[19] A. D. Martin, E. N. Ozmutlu, E. J. Squires, Nucl. Phys. B 121 (1997) 514.

[20] V. Srinivasan *et al.*, Phys. Rev. D 12 (1975) 681.

[21] L. Rosselet *et al.*, Phys. Rev. D 15 (1977) 574.

[22] G. Colangelo, J. Gasser and H. Leutwyler, Nucl. Phys. B 603 (2001) 125.

[23] BES Collaboration, M. Ablikim *et al.*,Phys. Lett. B 598 (2004) 149.

[24] S. Giovannella and S. Miscetti, KLOE Note 178 (2002).

[25] http://wwwasdoc.web.cern.ch/wwwasdoc/WWW/minuit/minmain/minmain.html .

[26] S. Eidelman et al., Phys. Lett. B 592 (2004).

[27] C. Gatti, M. Palutan and T. Spadaro, KLOE Note 209 (2006).